The influence of mantle plume in the genesis of the Cache Creek oceanic igneous rocks: implications for the geodynamic evolution of the inner accreted terranes of the Canadian Cordillera

Marc Tardy, Henriette Lapierre, L.C. Struik, D. Bosch, P. Brunet

The influence of mantle plume in the genesis of the Cache Creek oceanic igneous rocks: implications for the geodynamic evolution of the inner accreted terranes of the Canadian Cordillera

M. Tardy, H. Lapierre, L.C. Struik, D. Bosch, and P. Brunet

Abstract: West of Prince George, British Columbia, the Cache Creek Terrane is composed of mafic lavas interlayered with both mid-Permian pelagic limestones and Upper Triassic siliceous shales and greywackes. Gabbro, basalt, dolerites, and foliated clinopyroxene-rich ultramafic rocks are exposed within the Pinchi Fault system. The mid-Permian lavas show affinities of oceanic island tholeiites. Among the Triassic lavas, three types of rocks have been distinguished. Type 1 is geochemically similar to the mid-Permian volcanic rocks. Type 2 differs from type 1 by higher TiO_2 abundances and convex rare earth element patterns. Type 3 has the highest Zr, Nb, and Ta abundances and the greatest light rare earth element enrichment. The mafic rocks within the Pinchi Fault system are similar to N-type mid-ocean-ridge basalt (N-MORB), and the foliated ultramafic rocks are characterized by very low trace element contents, similar to extremely depleted harzburgites. Permian lavas and Triassic type 1 and igneous rocks from the Pinchi Fault system have the highest $\varepsilon_{Nd(i)}$ ratios (+7.4 to +9.6) and those of type 3 alkali have the lowest ratios (+2.0 to +5.3). The $\varepsilon_{Nd(i)}$ values of type 2 are intermediate between those of type 1 (~+7) and type 3 (~+4.9). This suggests that the Triassic rocks generated from a heterogeneous plume source or the mixing between depleted N-MORB and enriched oceanic island basalt sources. If the mafic igneous rocks sampled in central British Columbia are representative of the preserved parts of an oceanic crust, within the Cache Creek Terrane, then that crust was dominated by oceanic plateau components, perhaps due to the difficulty of subducting thick crust.

Résumé : À l'ouest de Prince George, en Colombie-Britannique, le terrane de Cache Creek est composé de laves mafiques interstratifiées avec des calcaires pélagiques du Permien moyen et des schistes argileux siliceux et des grauwackes du Trias supérieur. Dans le système de failles Pinchi, on retrouve des affleurements de gabbro, de basalte, de dolérite et de roches ultramafiques foliées et riches en clinopyroxène. Les laves du Permien moyen montrent des affinités avec des tholéiites d'îles océaniques. Parmi les laves du Trias, on distingue trois types de roches. La géochimie du type 1 est similaire à celle des roches volcaniques du Permien moyen. Le type 2 diffère du type 1 par de plus hautes concentrations de TiO_2 et des patrons convexes pour les éléments des terres rares. Le type 3 a les plus grandes concentrations de Zr, Nb, et Ta et le plus grand enrichissement en éléments de terres rares légers. Les roches mafiques à l'intérieur du système de failles Pinchi sont similaires aux basaltes médio-océaniques normaux (N-MORB) alors que les roches ultramafiques foliées sont caractérisées par de très faibles contenus en éléments traces, semblables à des harzburgites extrêmement appauvries. Les laves du Permien, les roches ignées et celles de type 1 du Trias provenant du système de failles Pinchi ont les rapports $\varepsilon_{Nd(i)}$ les plus élevés (+7,4 à +9,6) alors qu'ils sont les plus bas pour les roches alcalines de type 3 (+2,0 à +5,3). Les valeurs $\varepsilon_{Nd(i)}$ du type 2 sont intermédiaires entre celles du type 1 (~+7) et du type 3 (~+4,9). Cela suggère que les roches du Trias proviennent d'une source panache hétérogène ou d'un mélange entre des basaltes N-MORB appauvris et des sources enrichies de basaltes d'îles océaniques. Si les roches mafiques échantillonnées au centre de la Colombie-Britannique. sont représentatives de parties préservées d'une croûte océanique, à l'intérieur du terrane de Cache Creek, alors cette croûte a été dominée par des composantes du plateau océanique, peut-être parce qu'il eut été difficile à une croûte épaisse de passer en dessous d'une autre plaque.

[Traduit par la Rédaction]

Received February 29, 2000. Accepted October 25, 2000. Published on the NRC Research Press Web site on May 7, 2001. Paper handled by Associate Editor K. Andsell.

M. Tardy. Laboratoire de Géodynamique des Chaînes Alpines, UMR CNRS 5025, Université de Savoie, 73376 Le Bourget du Lac Cedex, France.
H. Lapierre.[1] Laboratoire de Géodynamique des Chaînes Alpines, UMR CNRS 5025, Université Joseph Fourier, Maison des géosciences, B.P. 53, 38041 Grenoble Cedex, France.
L.C. Struik. Geological Survey of Canada, 101-605 Robson Street, Vancouver, BC V6B 5J3, Canada.
D. Bosch. ISTEEM, Université de Montpellier 2, Pl. E. Bataillon, 34095 Montpellier Cedex 05, France.
P. Brunet. LMTG, UMR CNRS 5563, Université Paul Sabatier, 38 rue des trente-six ponts, 31400 Toulouse, France.

[1]Corresponding author (e-mail: tardy@univ-savoie.fr).

 DOI: 10.1139/cjes-38-4-515

Introduction

The Cache Creek Terrane lies between the Stikinia and Quesnellia arc terranes (Fig. 1) and belongs to an accretionary prism which extends from Yukon in the north to northern California in the south. This accretionary prism consists of tectonic slices of ultramafic and mafic igneous rocks, Triassic blueschists, pelagic to hemipelagic arc-derived sediments, and Upper Carboniferous to Lower Triassic platform carbonates which include a distinct Tethyan fusulinid and conodont fauna (Monger and Ross 1971; Orchard et al. 2001). Locally (as at Baker in Oregon and Cache Creek in British Columbia), the different components of this terrane occur as blocks (metre to kilometre scale) caught in a Permian to Triassic sheared argillaceous matrix.

According to the literature, the volcanic rocks which display features of oceanic plateau basalts are Late Carboniferous in age and form a sort of stable oceanic platform (Monger 1975; Souther 1991; Mihalynuk et al. 1994). Most of the Triassic mafic lavas are similar in composition to typical mid-oceanic-ridge basalts (MORB; Souther 1991) and represent the last vestige of perhaps 6000 km of consumed oceanic crust (Mihalynuk et al. 1994; Cordey and Struik 1996).

Here, we present mineral chemistry, bulk major and trace element concentrations, and Nd and Sr isotopic analyses of representative rock types from the Cache Creek Terrane exposed in the vicinity of Fort St. James (central British Columbia; Fig. 2A) and near Cache Creek type locality (Fig. 1). On the basis of these new geochemical data, we suggest that (*i*) the Cache Creek Terrane includes mid-Permian oceanic island basalts (OIB) and fragments of an Upper Triassic oceanic plateau and its associated oceanic lithosphere, and (*ii*) the Cache Creek Terrane is the result of collisions of oceanic plateau with arc in the Late Triassic.

Geologic setting and lithostratigraphic successions of the Cache Creek Complex

The Cache Creek Terrane in central British Columbia (Fig. 1) is bounded to the east by the Triassic Takla Group and Early Jurassic volcanic formations of the Quesnel Terrane (Quesnellia), and to the west by various units of the upper Paleozoic to Early Jurassic Stikine Terrane (Stikinia). These terranes represent oceanic and island arc suites accreted to the North American margin during the Mesozoic (Monger et al. 1972; Paterson 1973; Gabrielse and Yorath 1991).

Cache Creek Terrane in central British Columbia consists mostly of Upper Carboniferous to Lower Jurassic Cache Creek Complex, Permian to Lower Jurassic Sitlika assemblage (Paterson 1974; Childe and Schiarizza 1997; Schiarizza et al. 1998; Struik et al. 2001), and Upper Triassic to Lower Jurassic Tezzeron succession. The Triassic and Lower Jurassic metasedimentary Tezzeron succession comprises greywacke, sandstone, conglomerate, siltstone, and minor chert and limestone which are interpreted to be overlain by the ultramafic rocks exposed north of the west end of Pinchi Lake (Struik et al. 2001).

The northeastern part of the Cache Creek Terrane near Fort St. James (Figs. 2A, 2B, 4) is mainly composed of mid-Permian basalts interbedded with pelagic limestones and Upper Triassic pillowed and massive basalts and dolerites interlayered with siliceous shales, massive and brecciated cherts, greywackes, and slates (Sowchea succession; Struik et al. 1996). The contact between the Permian and Triassic rocks is not exposed.

Within the Pinchi Fault system are caught slices of (*i*) Upper Carboniferous to Permian platform carbonates (Mt. Pope succession), (*ii*) Upper Triassic blueschists, and (*iii*) undated rocks of mafic and ultramafic compositions. The mafic and ultramafic rock consists of layered cumulate gabbro with basaltic inclusions and intruded by fine-grained doleritic dykes; swarms of basaltic and doleritic dykes which crosscut fine-grained gabbros and dolerites (Rubyrock igneous complex); and foliated pyroxenite with Cr spinels bearing dunitic pods and lherzolite layers oriented parallel to the foliation (Trembleur Ultramafite, Murray Ridge; Figs. 2A, 2B, 3).

Feldspar porphyry dacite, lamprophyre, and diorite intrude these rocks as dykes and plutons, which locally cause a thermal metamorphism. The Cache Creek rocks are locally folded, cleaved, sheared, and brittlely faulted. In places, the ultramafic rocks form thrust sheets and klippes above the lower Mesozoic sediments (Struik et al. 2001).

Mid-Permian volcanic rocks are exposed at one locality (SCB95, PG96-2b, south of Fort St. James, Stuart Lake outlet; Figs. 2A, 2B, 4A). There, 1 m thick massive flows are interbedded with tuffs, volcaniclastic sediments, and lenses of micritic to bioclastic limestones which yielded mid-Permian conodonts (Orchard et al. 1998, 2001). The volcanic rocks have basaltic (PG96-2b) to icelanditic (SCB95) compositions (Table 1).

The Upper Triassic volcanic rocks crop out more extensively than the Permian basalts. However, they are poorly exposed because of the extensive Quaternary cover. Thus, the vertical and (or) lateral stratigraphic links between the different sequences are unknown. In most cases, the basalt occurs as massive flows, 1–3 m thick, interbedded with volcanic breccia, greywacke, and radiolarian cherts which yielded Late Triassic radiolarian faunas (Fig. 4B). Locally, coarse- to fine-grained breccias formed of basalt and chert fragments cemented by a siliceous matrix are interlayered within the cherts (Fig. 5). A few exposures of pillow basalts (PG96-1, PG97-20) and pillow breccias grading upwards into graded bedded lapilli and crystal tuffs have been observed.

Twenty-three representative samples of Sowchea succession, within the Pinchi Fault system, and melange near Cache Creek (Fig. 1) have been studied and analyzed to characterize the magmatic affinities of the igneous rocks.

Petrology and mineral chemistry of the mafic and ultramafic rocks

All the volcanic rocks of the Cache Creek Complex have undergone low-grade metamorphism. Plagioclase is replaced by albite, sericite, or less frequently by epidote. Olivine and orthopyroxene, where present, are replaced by smectites. Clinopyroxene is generally preserved but it may be replaced partly or totally by chlorite and (or) colourless actinolite or even pleochroic Mg-rich amphibole. Oxides are replaced by

Fig. 1. Simplified map of the accreted terranes of the setting between Quesnel and Stikinia (Canadian Cordillera), showing the location and geographic distribution of the Cache Creek Terrane.

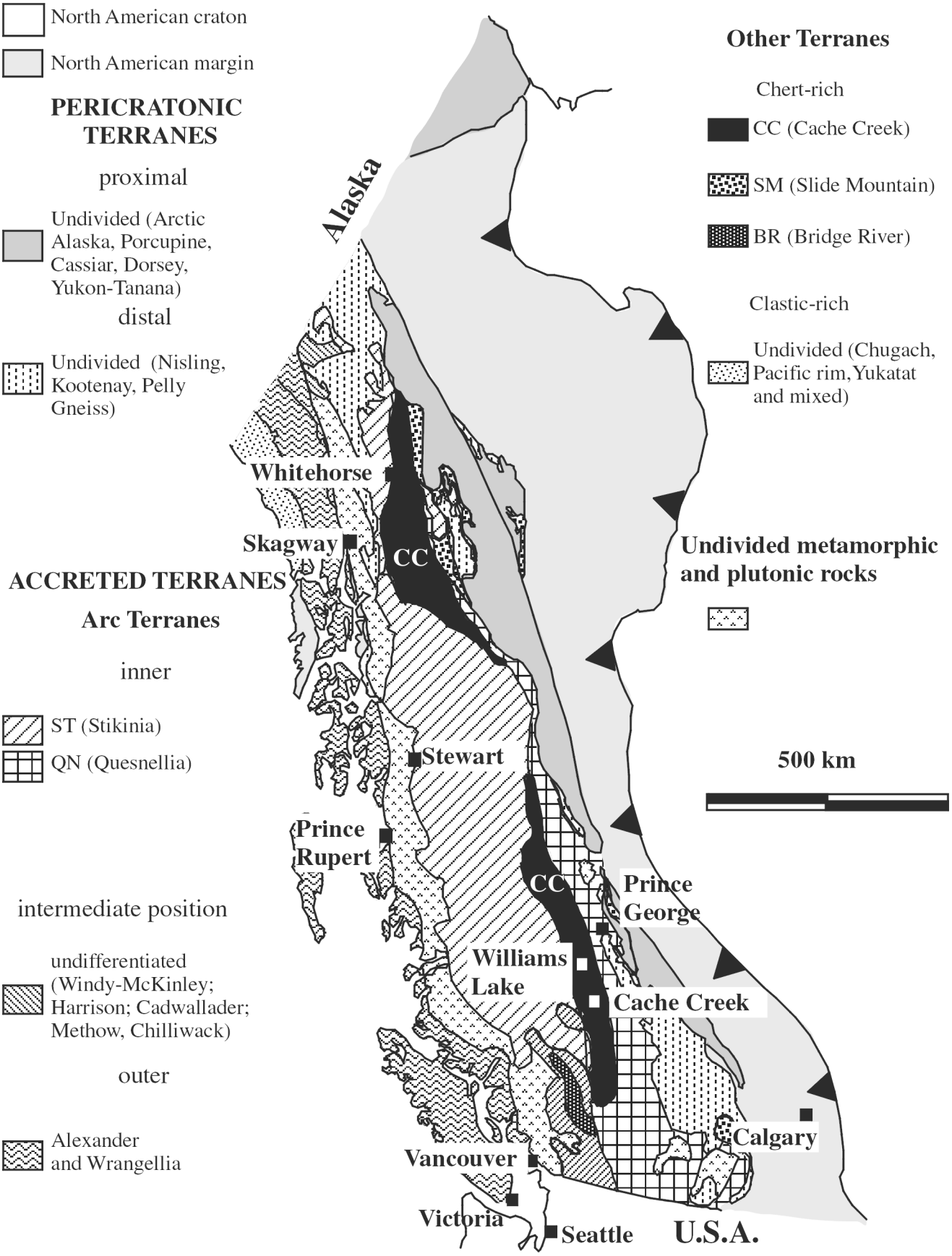

Fig. 2. (A) Simplified geological map of the Fort St. James area modified after Armstrong (1949) showing the location of the analyzed samples and cross section (see Fig. 3). In this area, the Pinchi strike-slip fault system separates the Cache Creek and Quesnel terranes. (B) Enlargement of the geological map in the Fort St. James area.

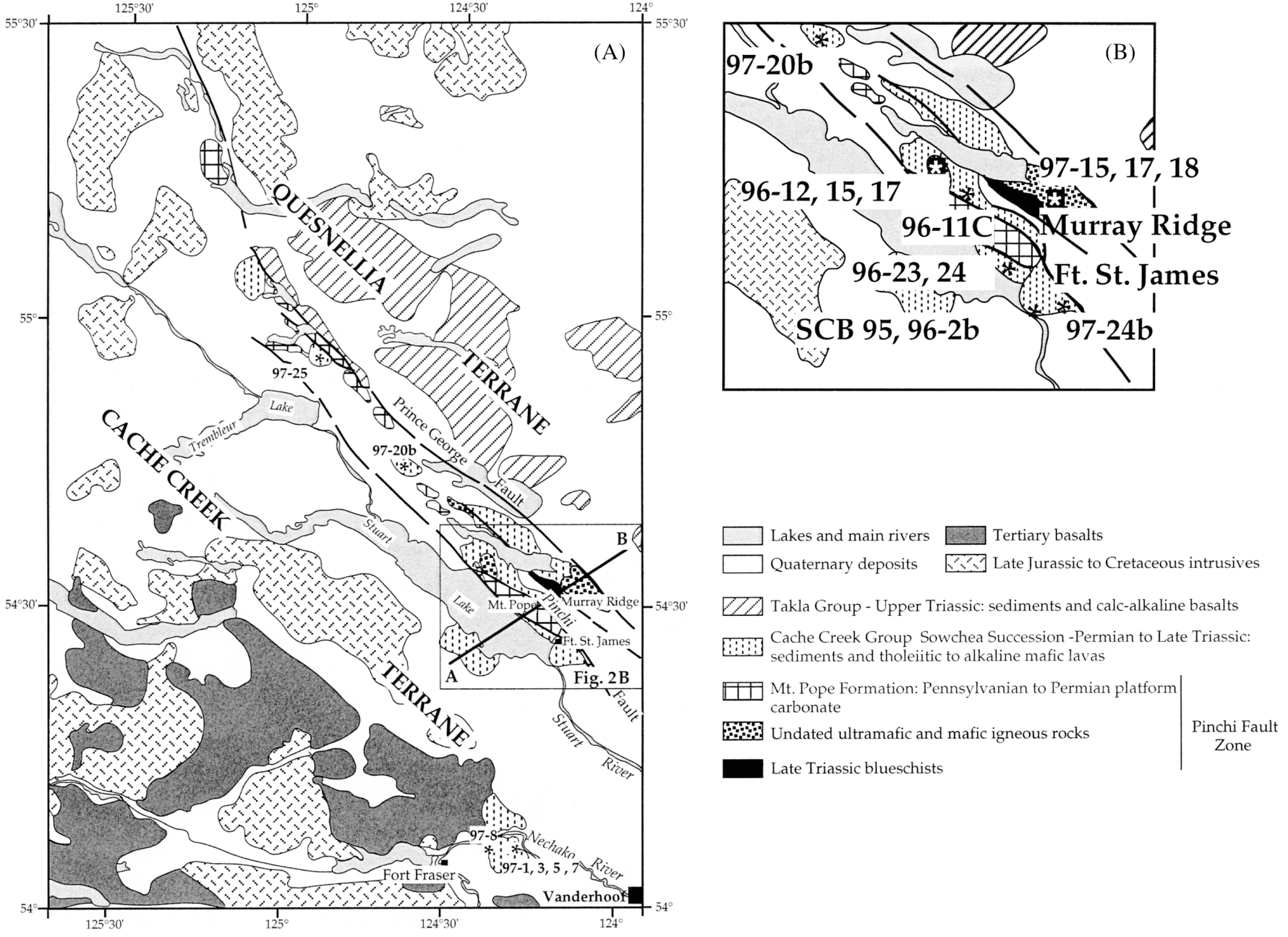

Fig. 3. Southwest–northeast cross section showing the tectonic relations between the Cache Creek and Quesnel terranes (location shown in Fig. 2A).

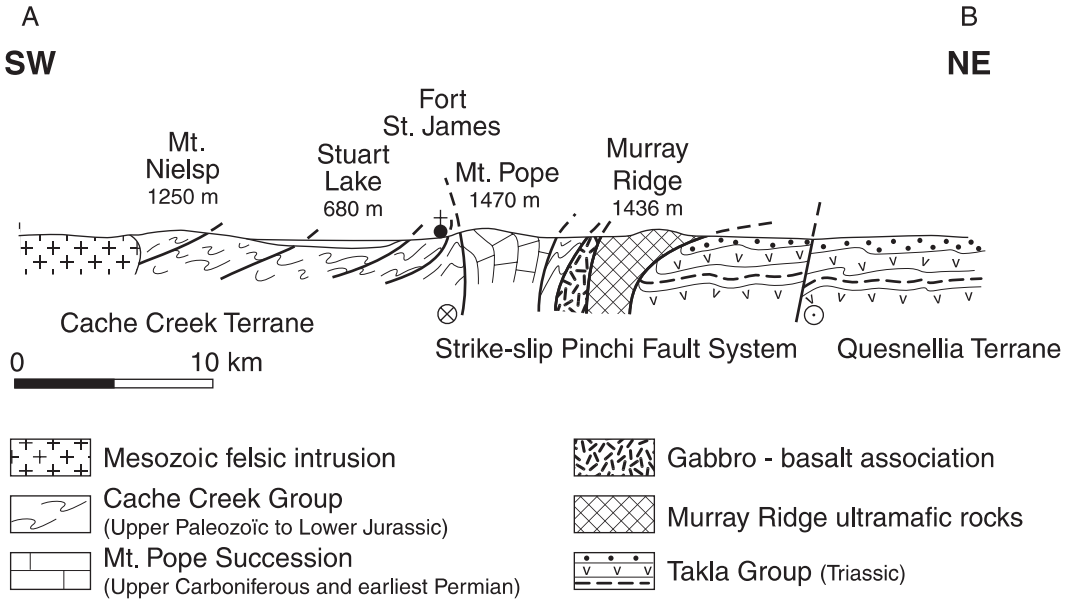

Fig. 4. Lithostratigraphic columns of (A) the Middle Permian and (B) the Upper Triassic – Lower Jurassic types 1 and 3 volcanic and sedimentary rocks of the Cache Creek Group. Refer to Figs. 2A and 2B for the location of the samples indicated in the columns and Table 1 for the volcanic rock types.

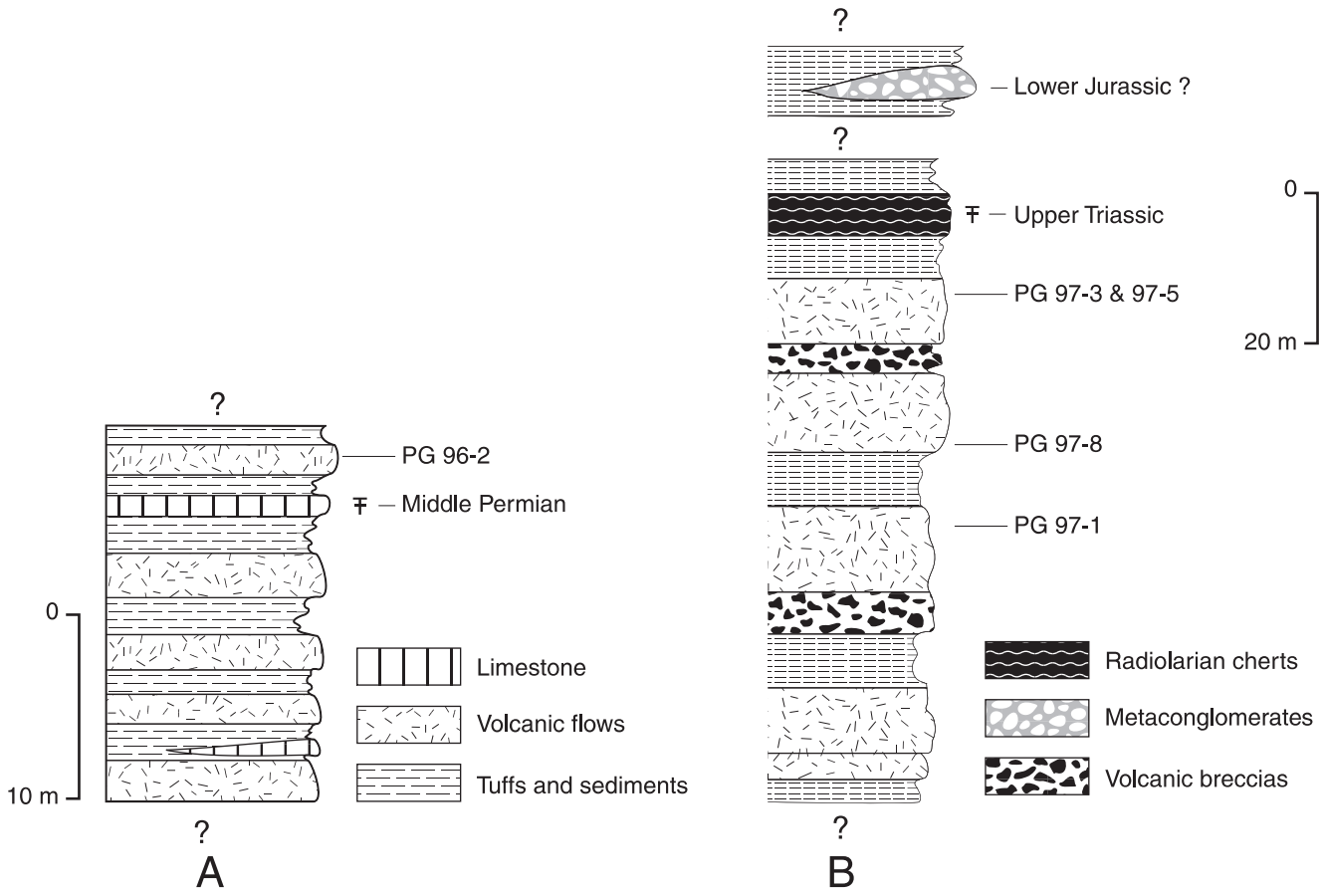

Table 1. Analytical data for selected Cache Creek Terrane igneous mafic rocks.

			Triassic					
	Permian		Type 1			Type 2		
Rock type:	Icelandite	Basalt	Basalt	Basalt	Basalt	Icelandite	Basalt	Basalt
Sample No.:	SCB95	PG96-2b	PG97-8	PG97-24	PG97-25	PG96-11c	PG96-23	PG96-24
SiO_2 (wt.%)	39.15	48.75	50.40	44.40	47.11	44.37	44.51	50.84
TiO_2	0.40	1.56	1.53	1.09	1.61	2.33	2.09	0.86
Al_2O_3	11.28	17.35	14.78	14.41	14.13	16.94	14.09	15.05
Fe_2O_3	15.70	10.15	10.92	11.42	13.88	14.82	12.63	7.74
MnO	0.24	0.12	0.17	0.02	0.21	.08	0.16	0.15
MgO	3.56	5.35	7.02	9.00	6.47	3.84	5.39	6.43
CaO	14.01	7.68	8.78	3.93	9.59	8.41	10.06	11.73
Na_2O	2.45	2.91	3.48	0.74	2.93	2.87	2.75	2.96
K_2O	1.04	2.56	0.52	5.37	0.38	1.28	0.63	1.88
P_2O_5	0.40	0.17	0.18	0.16	0.13	0.09	0.14	0.31
LOI	9.22	4.02	1.75	7.75	3.42	4.91	7.20	1.94
Total	99.60	100.62	99.49	99.58	99.86	99.94	99.65	99.89
Sc (ppm)		37.90	63.64	65.53	88.09	29.50	nd	31.70
V	220.35	296.70	503.08	426.86	675.71	248.90	nd	325.80
Cr	59.81	255.50	413.65	470.78	200.82	245.10	nd	226.40
Ni	26.25	52.11	95.89	132.49	70.56	186.40	nd	151.00
Rb	27.35	35.40	7.90	59.20	8.61	22.45	8.25	8.08
Sr	129.41	200.00	173.64	74.61	97.59	238.00	492.00	275.00
Ba	1637.11	243.00	57.05	277.04	326.50	38.48	32.20	22.79
U	0.17	0.39	0.16	0.42	0.10	0.24	0.76	0.17
Th	0.84	0.42	0.27	0.18	0.33	0.23	0.16	0.15
Pb	0.55	0.37	nd	nd	0.29	0.27	0.26	0.08
Hf	5.17	2.48	2.64	1.63	2.45	2.61	2.20	2.28
Zr	172.38	96.10	99.15	65.90	91.24	86.91	78.44	80.56
Ta	0.93	0.39	0.23	0.27	0.29	0.40	0.33	0.34
Nb	11.95	6.35	5.37	4.87	4.73	6.94	5.36	5.58
Y	41.49	29.95	36.99	20.14	31.90	19.76	26.77	26.33
La	9.08	5.33	4.82	3.80	4.54	3.15	4.04	3.96
Ce	24.80	14.09	14.52	10.57	12.81	12.72	14.02	13.57
Pr	3.87	2.23	2.32	1.57	1.99	1.99	2.60	2.53
Nd	19.68	11.05	11.98	7.56	10.38	10.62	13.79	13.47
Sm	6.19	3.53	3.86	2.33	3.40	3.38	4.10	4.14
Eu	2.17	1.27	1.37	0.92	1.32	1.19	1.39	1.40
Gd	7.90	4.30	4.59	2.83	4.36	3.58	4.40	4.35
Tb	1.42	0.75	0.88	0.51	0.77	0.62	0.43	0.75
Dy	9.04	4.86	5.70	3.29	5.04	3.81	4.48	4.51
Ho	1.92	1.06	1.27	0.73	1.11	0.78	0.92	0.93
Er	5.38	2.89	3.54	2.02	3.01	2.06	2.40	2.42
Tm	0.77	0.48	0.52	0.31	0.46	0.33	0.38	0.39
Yb	5.05	2.68	3.17	2.01	2.81	1.83	2.16	2.16
Lu	0.79	0.41	0.49	0.31	0.44	0.27	0.83	0.32
$^{87}Sr/^{86}Sr$			0.703531±13	0.715162±10	0.705630±14	0.705583±13	0.704797±11	
$^{87}Rb/^{86}Sr$			0.1316	2.2973	0.2552	0.2729	0.0850	
$(^{87}Sr/^{86}Sr)_i$[a]			0.70314	0.70830	0.70460	0.70477	0.70454	
εSr			–15.83	+57.48	+4.90	+7.31	+4.12	
$^{143}Nd/^{144}Nd$	0.513027±4	0.513524±8	0.513013±5	0.513091±10	0.513084±6	0.512986±6	0.512990±6	0.512876±6
$^{147}Sm/^{144}Nd$	0.19017	0.19315	0.19481	0.18635	0.19805	0.19243	0.18583	0.18582
$(^{143}Nd/^{144}Nd)_i$[a]	0.51270	0.51227	0.51275	0.51283	0.51281	0.51272	0.51273	0.51262
ε_{Nd}	+7.81	+9.61	+7.37	+9.12	+8.67	6.91	+7.16	+4.94

Note: Major element and Sc, V, Cr, and Ni analyses performed at the Université Claude Bernard, Lyon, France, and trace element analyses at the Université Joseph Fourier, Grenoble, France. LOI, loss on ignition; BIR, Icelandic Basalt.

[a] Analyses performed at the Université de Montpellier 2, Montpellier, France.

titanite. Vesicules are filled with calcite, chalcedony, or smectite ± pumpellyite ± zeolite. Glass is thoroughly replaced by smectite ± chlorite.

Cumulate gabbros are less altered than dolerites or mafic lavas. However, plagioclase is sometimes replaced by a microcrystalline association of epidote, quartz, and albite. Clinopyroxene is preserved but may be rimmed by Mg-rich pleochroic green hornblende. The foliated ultramafic rocks are remarkably preserved. However, olivine is sometimes serpentinized.

Table 1 (*continued*).

Triassic					
Type 3					
Basalt	Basalt	Basalt	Basalt	Basalt	Pillow
PG96-1	PG97-1	PG97-3	PG97-5	PG97-7	PG97-20b
47.53	47.08	47.50	44.33	45.35	45.29
1.55	2.23	3.33	2.78	2.66	3.03
13.97	10.38	14.25	17.13	16.35	13.92
9.55	9.70	13.58	12.09	12.34	13.28
0.17	0.26	0.17	0.17	0.15	0.15
7.53	5.59	6.43	3.82	4.28	7.43
11.53	13.14	7.11	8.67	10.01	8.74
3.42	1.33	3.18	3.18	3.41	3.07
0.34	1.19	1.10	1.53	0.50	0.51
0.16	0.44	0.45	0.60	0.56	0.54
4.48	7.80	3.03	4.07	2.90	3.45
100.15	99.14	100.13	99.45	99.51	99.90
32.30	35.60	48.45	47.55	47.21	49.67
240.60	411.36	666.41	739.63	666.34	526.25
244.60	23.04	66.27	24.81	22.22	436.01
92.30	22.215	44.525	19.70	15.39	130.25
4.19	27.93	16.03	16.55	6.09	10.59
142.00	209.80	326.59	411.33	458.81	153.92
61.89	479.11	275.84	346.76	197.32	85.13
0.36	0.53	0.81	1.06	0.80	1.05
0.62	2.16	2.44	2.66	2.46	3.53
0.50	4.62	0.23	0.70	0.32	0.55
2.48	4.41	5.49	5.44	5.05	7.73
97.14	188.04	239.15	235.60	214.67	335.55
0.62	1.60	2.22	2.62	2.38	2.68
9.20	26.53	36.41	42.09	37.98	45.25
21.89	26.81	33.32	39.17	34.08	35.21
7.87	22.98	28.46	29.19	26.84	30.24
19.64	49.55	61.62	66.91	62.10	73.87
2.84	6.17	7.75	8.58	7.90	9.72
12.71	26.16	32.96	37.18	33.91	43.05
3.44	5.99	7.39	8.39	7.77	9.88
1.15	1.81	2.56	2.72	2.53	3.08
3.80	6.27	7.55	8.78	7.83	9.55
0.61	0.87	1.10	1.27	1.15	1.36
3.83	4.69	5.83	6.91	6.19	6.82
0.79	0.95	1.15	1.38	1.24	1.25
2.09	2.42	2.86	3.42	3.06	2.85
0.33	0.35	0.40	0.48	0.43	0.38
1.90	2.08	2.35	2.76	2.50	2.10
0.28	0.32	0.35	0.42	0.37	0.30
	0.706800±13	0.704008±11	0.704211±11		0.703825±8
	0.3851	0.1420	0.1164		0.1990
	0.70565	0.70358	0.70386		0.70323
	+19.83	–9.50	–5.53		–14.52
0.512865±6	0.51266±3	0.512788±5	0.512778±4	0.512784±4	0.512823±6
0.16376	0.13843	0.13555	0.13875	0.13853	0.13875
0.51264	0.512247	0.51260	0.51259	0.51259	0.51263
+5.31	+1.99	+4.57	+4.35	+4.41	+5.17

Volcanic rocks of the Sowchea succession

The mid-Permian suite includes intersertal basalt and icelandite. The intersertal basalt (PG96-2b; Figs. 2A, 2B) consists of plagioclase phenocrysts (less than 1 mm size) enclosed in an intersertal groundmass formed of zoned augite, late-crystallizing Ti magnetites, and interstitial pumpellyite. The icelandite (SCB95) differs from the basalt by the absence of phenocrysts and the presence of abundant calcite-filled vesicles. The groundmass is formed of flow-aligned plagioclase microlites and Fe–Ti oxides.

Table 1 (*concluded*).

	Pinchi Fault (undated)							
Rock type:	Dolerite	Dolerite	Basalt	Gabbro	Ultramafic	Pyroxenite	Clinopyroxene	
Sample No.:	PG96-15	PG96-17	PG96-12	PG96-14	SH903b[a] (ppb)	PG97-17	PG97-17	BIR standard
SiO_2 (wt.%)	52.70	48.72	45.93	48.98				
TiO_2	0.46	1.75	1.90	0.29				
Al_2O_3	14.23	14.66	14.75	21.30				
Fe_2O_3	9.25	13.56	14.23	4.93				
MnO	0.16	0.21	0.23	0.08				
MgO	9.17	5.63	5.88	5.72				
CaO	8.14	9.56	10.64	12.41				
Na_2O	3.32	3.04	2.41	2.71				
K_2O	0.10	0.12	0.04	0.14				
P_2O_5	0.05	0.15	0.19	0.09				
LOI	2.61	2.89	2.52	3.27				
Total	100.19	100.29	98.70	99.92				
Sc (ppm)	62.31	98.37	nd	162.06				
V	412.53	793.50	500.00	162.06		61.0		
Cr	723.22	107.64	66.10	434.59		3330.0		
Ni	148.35	31.20	nd	89.285		892.0		
Rb	1.26	0.448	0.585	0.846	168.00	0.1322	0.1378	0.33
Sr	117.90	73.437	115.506	229.704	471.00	0.933	0.9874	114.03
Ba	61.48	10.147	53.445	45.169	1780.00	9.598	12.398	8.37
U	0.04	0.082	0.010	0.028	5.70	0.057	0.0041	0.11
Th	0.06	0.186	0.014	0.043	17.20	0.0085	0.011	0.03
Pb	nd	0.463	0.335	0.316	132.00	0.633	0.1493	4.06
Hf	0.67	1.239	0.607	0.752	3.00	0.0105	0.0039	0.62
Zr	21.10	25.501	13.834	20.892	77.90	0.3596	0.1414	15.73
Ta	0.03	0.165	0.152	0.030	1.30	0.0012	0.001	0.05
Nb	0.88	2.678	2.796	2.022	24.30	0.2672	0.0587	0.59
Y	12.21	44.374	34.082	13.553	nd	0.0669		16.73
La	0.82	3.909	1.877	1.386	27.60	0.025	0.2360	0.64
Ce	2.41	12.666	6.730	3.963	63.10	0.057	0.0551	2.00
Pr	0.41	2.241	1.350	0.666	7.70	0.0064	0.00616	0.38
Nd	2.08	11.884	8.215	3.557	28.90	0.023	0.2478	2.45
Sm	0.83	4.215	3.210	1.221	8.10	0.0046	0.0045	1.08
Eu	0.34	1.504	1.467	0.609	1.50	0.0017	0.0004	0.52
Gd	1.19	5.394	4.563	1.715	7.20	0.0057	0.0523	1.75
Tb	0.25	0.993	0.820	0.317	1.10	0.001	0.00772	0.36
Dy	1.77	6.448	5.408	2.102	7.30	0.0075	0.00675	2.51
Ho	0.42	1.428	1.171	0.464	2.00	0.002	0.00187	0.59
Er	1.28	4.010	3.190	1.314	8.40	0.0092	0.0080	1.68
Tm	0.20	1.898	2.265	1.666	1.80	nd	nd	nd
Yb	1.33	3.875	3.024	1.221	15.40	0.0196	0.00181	1.59
Lu	0.22	0.579	0.462	0.188	3.40	0.0042	0.0039	0.25
$^{87}Sr/^{86}Sr$	0.703097±7	0.704508±7	0.703294±12	0.702985±11				
$^{87}Rb/^{86}Sr$	0.0309	0.0176	0.0158	0.0107				
$(^{87}Sr/^{86}Sr)_i$[a]	0.70300	0.70445	0.70325	0.70295				
εSr	–17.73	+2.87	–14.24	–18.46				
$^{143}Nd/^{144}Nd$	0.513101±7	0.513092±6	0.513149±6	0.513066±8				
$^{147}Sm/^{144}Nd$	0.24127	0.21427	0.23902	0.20621				
$(^{143}Nd/^{144}Nd)_i$[a]	0.51277	0.51279	0.51282	0.51278				
ε_{Nd}	+7.84	+8.39	+8.84	+8.10				

Three types have been distinguished among the Upper Triassic lavas. This distinction is based on the mineralogy; sequence of crystallization; MgO, Cr, and V contents; and rare earth element patterns (REE) (refer to Table 1 and Fig. 8). Type 1 is characterized by the highest MgO (>6.5%), Cr (>200 ppm), and V (>426 ppm) abundances and flat rare earth patterns. Type 2 differs from type 1 by lower MgO (<6.5%) contents and REE patterns depleted in La and Ce relative to Sm. Type 3 differs from both types 1 and 2 by variable MgO contents, significantly higher Zr and TiO_2 abundances, and light rare earth element (LREE) enriched patterns relative to heavy rare earth element (HREE). Types 1 and 2 are tholeiitic and type 3 is alkalic.

Type 1 consists of aphyric (PG97-8, PG97-24; Figs. 2A,

Fig. 5. Northeast–southwest cross section observed along the trail leading to Mount Pope, showing the tectonic relations between the Upper Carboniferous – earliest Permian limestone of the Mount Pope Formation and possible Upper Triassic polymictic breccia (type 2 basalt and chert fragments). R, Recent.

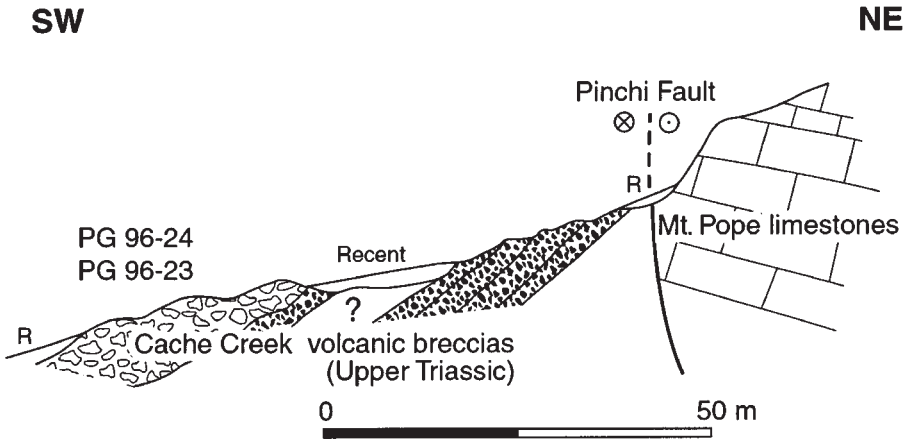

2B) or intersertal (PG97-25; Fig. 2A) basalts. The aphyric basalts exhibit quenched clinopyroxene and plagioclase crystals (0.1–0.5 mm) set in a vesicular glassy groundmass now replaced by smectites and chlorites. The vesicles are filled with chalcedony ± calcite ± smectites ± pumpellyite. The intersertal basalts (PG97-25) are composed of 1 mm sized plagioclase laths (40%) embedded in clinopyroxene (50%), Ti-magnetite (10%), and a silicified groundmass. Plagioclase is an albite ($An_{90–95}$) and clinopyroxene has a Ti-poor augite ($Wo_{39–32}$, $En_{35–47}$, $Fs_{13–32}$) composition (Table 2; Fig. 6). Within the sample, clinopyroxene composition displays a FeO enrichment correlated with a MgO depletion, whereas CaO remains constant.

Type 2 (PG9611C, PG96-23, PG96-24; Figs. 2A, 2B, 5) consists of aphyric basalts and icelandites which are the most vesicular and altered lavas of the suite. Clinopyroxene is most commonly replaced by colourless actinolite and plagioclase by albite. The vesicles are filled by calcite rimmed by smectites, pumpellyite, and clinozoisite.

Type 3 displays intersertal texture in the massive flows or pillow cores. The best preserved lava (PG97-25; Fig. 2A) consists of 1 mm sized euhedral plagioclase laths (50%) surrounded by clinopyroxene (40%), magnetite (15%), and glass presently replaced by green pleochroic smectites. Clinopyroxene cores are generally colourless and the rims are pink and pleochroic. The cores are TiO_2-poor (<0.5%) augites ($Wo_{35–29}$, $En_{39–35}$, $Fs_{31–29}$; Table 2; Fig. 6), and the rims are TiO_2-rich (3–4.5%) diopsides ($Wo_{47–48}$, $En_{31–35}$, $Fs_{19–21}$; Table 2; Fig. 6). When preserved, plagioclase is an oligoclase (Ab_{70}). Most frequently, it shows an albite composition ($Ab_{96–98}$). When aphyric, the petrography of type 3 is similar to that of type 2.

Mafic rocks within the Pinchi Fault system

Phyric basalt (PG96-12; Fig. 2B) included in cumulate layered gabbro (PG96-14) consists of centimetre-long plagioclase and clinopyroxene phenocrysts set in an ophitic groundmass composed of plagioclase (50%) laths (up to 5 mm long) cemented by anhedral clinopyroxene (30%) and Fe–Ti oxides (10%). Where preserved, plagioclase composition ranges from andesine to labradorite ($An_{40–55}$). Ti- and Cr-poor clinopyroxene composition ranges from diopside ($Wo_{45–46}$, $En_{36–39}$, $Fs_{18–25.5}$) to augite ($Wo_{37–45}$, $En_{37.5–38}$, $Fs_{18–25.5}$; Table 2; Fig. 6).

The fine-grained gabbro (PG96-14; grain size <1 cm) consists of adcumulate euhedral plagioclase (50%) embedded by (30%) Mg-rich augite ($Wo_{43–46}$, $En_{37–38}$, $Fs_{16.5–25}$; Table 2; Fig. 6) and (10%) orthopyroxene. Green pleochroic hornblende (10%) rims clinopyroxene grains or occurs as pseudomorphs after clinopyroxene.

Fine-grained dolerite dykes (PG96-15) intruding the gabbro consist of 1 mm long plagioclase ($An_{45–6}0$) laths (60%) embedded in green pleochroic hornblende (40%) and late-crystallizing magnetite (10%). Scapolites and epidote-filled veinlets may occur.

The doleritic dykes from the Rubyrock igneous complex (PG96-17; Fig. 2B) differ from the previously described dolerite by porphyritic texture and the presence of smectites and chlorites pseudomorphs after orthopyroxene and interstitial quartz.

The very well preserved ultramafic rocks from Murray Ridge consist of foliated pyroxenites, lherzolites, and dunites. Pyroxenites and lherzolites are coarse grained, with significant recrystallization of the olivine and pyroxenes giving aggregates of mosaic-shaped grains flattened parallel to the foliation. These rocks contain approximately 1–10% of Cr spinel. The picotite crystals are systematically euhedral.

Pyroxenite (PG97-17) consists predominantly of clinopyroxene (80%) and orthopyroxene (less than 20%). Orthopyroxene composition is very homogeneous ($Wo_{1.4–2.6}$, $En_{90–88}$, $Fs_{10–8}$; Table 2; Fig. 6), whereas clinopyroxene shows a wider range of composition. Diopside ($Wo_{46–48}$, En_{50}, Fs_3) is the most common type. However, some clinopyroxenes have augite (Wo_{33}, En_{63}, Fs_4) or pigeonite ($Wo_{9–6}$, $En_{88–91}$, Fs_3) compositions.

Lherzolite (PG97-18) is composed of Ni-poor olivine (80%; $Fo_{91–92}$; Table 2; Fig. 6), diopside (10%, $Wo_{\sim 47}$, $En_{\sim 50}$, $Fs_{\sim 3}$; Table 2; Fig. 6), and orthopyroxene (10%), the composition of which is very similar to that of the pyroxenite ($Wo_{1.5–2}$, $En_{\sim 90}$, $Fs_{7–8}$; Fig. 6).

Fosterite (Fo_{92}) is the main component (95%) of dunite

Table 2. Representative clinopyroxene, orthopyroxene, olivine, and Cr spinel analyses.

(A) Clinopyroxene and orthopyroxene

	Cache Creek Formation						Pinchi Fault system			
	Type 1			Type 3			Basalt			Gabbro
Sample No.:	PG97-25	PG97-25	PG97-25	PG97-3	PG97-3	PG97-3	PG96-12	PG96-12	PG96-12	PG96-14
SiO_2 (wt.%)	54.00	53.48	51.43	54.08	42.77	44.31	51.71	48.07	52.22	48.29
TiO_2	0.47	0.53	0.88	0.03	4.52	4.22	0.28	0.20	0.33	1.80
Al_2O_3	1.49	2.31	1.49	3.08	8.29	7.31	1.47	3.99	1.66	7.95
Cr_2O_3	0.00	0.10	0.00	0.00	0.12	0.10	0.09	0.06	0.10	0.22
FeO[a]	11.46	8.32	19.94	16.47	11.82	11.51	11.23	15.71	11.00	11.89
Fe_2O_3										
MnO										
MgO	16.88	16.95	11.94	11.81	9.98	10.58	12.77	13.26	12.88	15.34
CaO	17.32	19.70	15.43	11.91	21.66	21.62	21.09	18.02	21.90	11.47
Na_2O	0.24	0.20	0.86	0.89	0.63	0.53	0.36	0.16	0.34	2.33
K_2O	0.01	0.02	0.00	0.11	0.00	0.00	0.00	0.00	0.01	0.12
Total	101.88	101.69	101.98	98.37	99.98	100.18	99.00	99.47	100.45	99.41
Wo	34.8	39.6	32.4	28.9	48.4	47.7	44.3	37.0	45.2	27.3
En	47.2	47.4	34.9	39.9	31.0	32.5	31.3	37.9	37.0	50.7
Fs	18.0	13.1	32.7	31.2	20.6	19.8	18.4	25.2	17.7	22.0
Mg#	0.72	0.78	0.47	0.93	0.93	0.89	0.67	0.60	0.67	0.69

(B) Olivine and Cr spinel

	Olivine				Cr spinel					
	Lherzolite		Dunite		Dunite			Lherzolite		
	PG97-18	PG97-18	PG97-15	PG97-15	PG97-15	PG97-15	PG97-15	PG97-18	PG97-18	PG97-18
SiO_2 (wt.%)	41.44	40.86	41.53	41.08	0.02	0.04	0.02	0.02	0.04	0.00
TiO_2	0.00	0.00	0.07	0.00	0.02	0.06	0.08	0.09	0.05	0.09
Al_2O_3	0.02	0.00	0.06	0.00	17.07	16.99	19.04	13.76	13.35	13.34
Cr_2O_3	0.01	0.00	0.03	0.07	50.41	50.76	47.78	56.10	56.53	58.07
FeO[a]	7.81	8.17	8.43	7.98	16.70	16.80	17.46	19.01	18.69	16.82
Fe_2O_3					3.41	2.98	3.72	0.50	1.12	0.27
MnO					0.61	0.71	0.59	0.74	0.75	0.65
MgO	51.70	51.04	49.33	50.75	11.32	11.22	10.64	9.48	9.75	11.02
CaO	0.00		0.06	0.08						
Na_2O	0.00		0.03	0.00						
K_2O	0.00		0.04	0.00						
Total	100.97	100.08	99.36	99.96	99.57	99.55	100.46	99.71	100.28	100.26
Fo	92.2	91.8	91.3	91.9						
Fa	7.8	8.2	8.7	8.1						
Cr					1.273	1.212	1.282	1.452	1.455	1.482
Al					0.643	0.64	0.64	0.531	0.512	0.507
Cr#					0.66	0.66	0.63	0.734	0.73	0.74
Mg#					0.50	0.506	0.487	0.466	0.47	0.48
Fe^{3+}/SFe					0.186	0.187	0.057	0.042	0.053	0.0154

Note: Microprobe analyses performed on a CAMEBAX at the University of Lausanne, Lausanne, Switzerland. Conditions of analysis: 15 kV, 10–20 nA, focused beam, natural standards. Fe_2O_3 calculated assuming $Fe^{3+} = 16 - ((2(Ti^{4+}) + Al^{3+} + Cr^{3+}) \times 24/(\text{Sum Cat}))$.

(PG97-15), and picotite is slightly more abundant (5%) than in the clinopyroxene-bearing ultramafic rocks.

Representative picotite analyses are presented in Table 2 and a plot of Cr# (molar Cr/(Cr + Al)) versus Mg# (molar Mg/(Mg + Fe)) is shown in Fig. 7. Cr# ranges from 0.56 to 0.74. In a plot of Cr# versus Mg#, these spinels plot between the dunite and harzburgite fields, with the exception of those of the pyroxenite which are displaced to the right of the diagram towards higher Mg#. These spinels appear to be more Al_2O_3 depleted than those of abyssal peridotites. Remarkably, spinels in lherzolite are more Al_2O_3 depleted ($0.75 < Cr# < 0.71$) than those occurring in pyroxenite ($0.74 < Cr# < 0.56$) or dunite ($0.71 < Cr# < 0.62$).

Several authors (Dick and Bullen 1984; Bonatti and Michael 1989; Arai 1994) have used the composition of mineral phases to constrain the degree of partial melting and likely tectonic settings of peridotites. Figures 7B and 7C are plots of spinel Cr# versus Mg# in olivine and Al_2O_3 content of orthopyroxene. Orthopyroxene analyses from the peridotites cluster within the subduction zone related peridotite field. In many ultramafic assemblages there is a good inverse correlation between Cr# and Al_2O_3 of orthopyroxene. For the Murray Ridge peridotites, this correlation is not present, and all the samples plot at the depleted end of the subduction zone related peridotite field. Moreover, lherzolite spinels appear to be even more depleted than those of dunite.

Table 2. (*concluded*).

Pinchi Fault system												
Gabbro		Pyroxenite							Lherzolite			
PG96-14	PG96-14	PG97-17	PG97-17	PG97-17	PG97-17	PG97-17	PG97-17	PG97-17	PG97-18	PG97-18	PG97-18	PG97-18
48.16	48.11	54.08	53.98	54.66	54.57	58.04	57.39	56.93	54.66	54.93	57.98	57.23
1.92	1.78	0.00	0.00	0.02	0.05	0.01	0.06	0.05	0.03	0.03	0.00	
8.14	9.18	1.04	1.11	0.61	0.72	0.54	0.64	0.61	0.66	0.87	0.79	0.66
0.06	0.09	0.64	0.73	0.68	0.67	0.42	0.51	0.41	0.29	0.62	0.31	0.45
11.85	12.17	2.89	2.11	1.97	2.21	6.47	5.64	5.33	1.85	1.89	5.43	6.42
				0.10	0.06	0.15	0.19	0.19		0.05		0.16
15.32	14.72	23.64	18.21	17.71	18.07	34.18	33.47	32.28	18.59	18.34	35.42	34.17
11.78	11.61	17.21	23.69	24.21	23.72	0.73	1.76	3.64	24.08	23.57	0.90	0.70
1.83	1.73	0.12	0.19	0.09	0.11	0.01	0.03	0.02	0.15	0.14	0.00	0.00
0.14	0.10	0.02	0.01	0.00	0.00	0.00	0.00	0.00	0.00	0.00	0.00	0.00
99.21	99.50	99.66	100.03	100.06	100.20	100.55	99.69	99.46	100.32	100.45	100.82	99.78
27.8	27.9	32.9	46.8	48.048	46.951	1.900	3.307	6.875	46.900	46.617	1.600	1.373
50.3	49.2	62.8	50.0	48.894	49.770	88.900	87.491	84.811	50.300	50.464	90.600	89.288
21.8	22.8	4.3	3.3	3.057	3.279	9.200	9.202	8.314	2.800	2.919	7.800	9.406
0.70	0.68	0.34	0.93	0.83	0.93	0.90	0.90	0.90	0.94	0.94	0.92	0.96

Cr spinel		
Pyroxenite		
PG97-17	PG97-17	PG97-17
0.00	0.00	0.03
0.04	0.04	0.08
12.25	13.66	13.80
53.79	53.42	52.61
23.51	21.52	22.78
2.54	2.35	2.50
0.78	0.75	0.75
6.16	7.70	6.94
99.06	99.44	99.49
1.443	1.404	1.389
0.49	0.535	0.543
0.74	0.72	0.72
0.29	0.36	0.36
0.097	0.098	0.099

The volcanic blocks of the Cache Creek Melange

In southern British Columbia, at the Cache Creek type locality, and in the vicinity of Williams Lake (Fig. 1), the different components of the Cache Creek accretionary prism occur as blocks (metre to kilometre scale) caught in a Permian to Triassic sheared argillaceous matrix. The blocks consist of Permian reef limestones, serpentinites, sheared volcaniclastic sediments, mudstones, and mafic lavas.

Petrological and geochemical data of samples collected in the melange show that these volcanic blocks are similar to the Upper Triassic lavas of the Sowchea succession exposed near Fort St. James (Fig. 10; Table 3).

Samples 95CC1 and 95CC4 from near the Cache Creek locality are aphyric basalts with abundant albite quenched microphenocrysts and microlite pseudomorphs after plagioclase. The groundmass of these basalts is replaced by smectites and chalcedony, and includes calcite–smectites-filled vesicules (~1 mm size).

Sample 99WL7 is from a highly vesicular basaltic block exposed 35 km north of Williams Lake along Highway 97. It is formed of abundant flow-aligned plagioclase phenocrysts and microlites set in a highly vesicular groundmass. Plagioclase is replaced by smectites and Fe–Ti oxides by titanite. The large vesicules are filled with calcite, smectites, chlorite, and zeolites.

Sample 99WL2 was collected south of Williams Lake (Fig. 1). It is an intersertal basalt composed of microphenocrysts (<1 mm size) of albite and actinolite pseudomorphs after

Fig. 6. Major element compositions of pyroxene and olivine of Cache Creek types 1 and 3 basalt (Sowchea succession) and mafic and ultramafic rocks (Murray Ridge) from the Pinchi Fault system. Pyroxene nomenclature after Morimoto (1988).

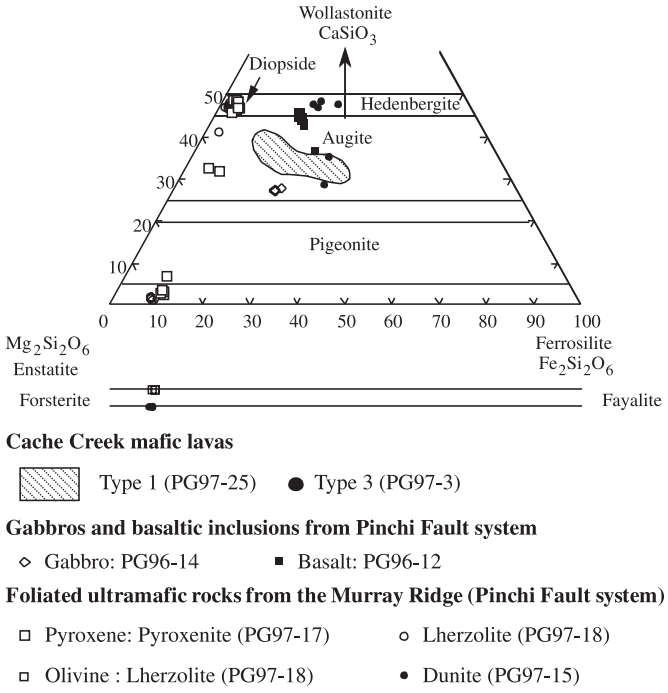

clinopyroxene, acicular magnetite, calcite ± smectites filled amygdules caught in a groundmass recrystallized into smectites ± chlorite. Samples 99WL5 and 99WL6 were collected 25 km north of Williams Lake, on Highway 97, a few kilmometres south of McLeese Lake. Both rocks have aphyric textures and consist of an epidote-rich groundmass which includes sparse albite microlites and abundant large vesicules filled with calcite + pumpellyite ± smectites.

Finally, dolerites 99CC1 and 99CC2 were collected north of the Cache Creek locality, at the junction of highways 99 and 97N. These rocks are intensely fractured and altered. Clinopyroxene is totally replaced by colourless actinolite, and plagioclase is albitized. Fractures are filled with smectites and quartz.

Geochemistry of the mafic and ultramafic rocks

Representative whole rock major, trace element, and Nd and Sr isotopic chemistry of the Cache Creek lavas and igneous and metamorphic rocks from the Pinchi Fault are represented in Tables 1 and 3. Because of the low-grade metamorphism which affects the Cache Creek Complex igneous rocks, large ion lithophile elements (LILE; Ba, Rb, Sr, K, Ba, U, and Pb) known to be sensitive to alteration and metamorphism will not be considered representative of the primary composition of these rocks.

Analytical procedures

Trace elements were analyzed at the University of Grenoble by inductively coupled plasma – mass spectrometry (ICP–MS, VG-PQ^{2+}), after acid dissolution, using procedures of Barrat et al. (1996). Trace element analyses of the foliated ultramafic rocks were performed by ICP–MS (VG-PQ^{2+}) at Université de Montpellier. Standards used for the analyses were JB2, WSE, BIR-1, JR1, BHVO, and UBN. Major element and compatible trace element analyses were performed by X-ray fluorescence spectrometry (XRF) at Université Claude-Bernard at Lyon or by ICP – optical emission spectroscopy at the Centre Recherches Pétrographique et Géochimique (CRPG) de Nancy.

Volcanic rocks of the Sowchea succession

The primitive mantle normalized (Sun and McDonough 1989) plots of the Permian basalt and icelandite (Fig. 8A) are similar to those of intraoceanic island tholeiite (OIT). Their REE patterns are slightly enriched in LREE ($1.3 < (La/Yb)_N < 1.5$). Their Zr/TiO_2 ratios are higher than those of oceanic plateau basalts (OPB), given as reference (Ontong Java, Neale et al. 1997; Caribbean–Colombian, Kerr et al. 1997) at similar Nb/Y (~0.2, Fig. 9A).

Type 1 Triassic basalts are geochemically similar to the Permian basalt, (i.e., $1.1 < (La/Yb)_N < 1.4$; $0.8 < (La/Sm)_N < 1.05$), but their Zr/TiO_2 values are lower and similar to those of OPB (Figs. 8B, 9A).

Type 2 consists of basalt and icelandite and is geochemically distinct from type 1 by higher TiO_2 and Ni abundances and convex REE patterns ($(La/Sm)_N = 0.6$; Fig. 8C). The icelandite differs from the basalts by higher Nb/Y and lower Zr/TiO_2 ratios (Fig. 9A).

Among the mid-Permian and Upper Triassic tholeiitic lavas of the Sowchea succession, type 1 resembles most the Ontong Java plateau basalts (Fig. 8).

Type 3 is composed of basalt and hawaiite and has the highest Zr, Nb, and Ta contents and the greatest LREE enrichment ($7.6 < (La/Yb)_N < 10.3$; $(La/Sm)_N = 2$). Their hump-shaped primordial mantle (PM) normalized multielement patterns are typical of those of alkali lavas (Fig. 8D). They differ from the mid-Permian and Upper Triassic types 1 and 3 volcanic rocks by significantly higher Nb/Y and lower Zr/TiO_2 ratios, which fall in the range of alkali basalts.

Figure 9B is a Zr/Y versus Zr/Nb plot illustrating the variable degrees of partial melting of the volcanic rocks of the Sowchea succession. Relative to the southern Pacific Rise MORB (Mahoney et al. 1994), the mid-Permian and Upper Triassic tholeiites display, like the Ontong Java basalts, a very restricted range of Zr/Nb values consistent with high degrees of partial melting (Nb being highly incompatible and Zr moderately incompatible during melting). The alkali type 3 basalt and hawaiite differs from the tholeiite by higher Zr/Y and $(La/Yb)_N$ ratios (Fig. 9C). Conversely, the Zr/Y and $(Dy/Yb)_N$ ratios of the Upper Triassic alkali volcanic rocks are lower than those of the Cache Creek tholeiite and Ontong Java plateau basalt.

Ultramafic and mafic rocks within the Pinchi Fault system

Basalt (PG96-12), dolerite (PG96-15), and gabbro (PG96-14) from the Pinchi Fault system (Figs. 2A, 2B) are depleted in LREE ($0.4 < (La/Yb)_N < 0.88$) and in Zr, Hf, and Th, rela-

Fig. 7. Plots of Cr# (molar Cr/(Cr + Al)) for spinels versus (A) Mg# (molar Mg/(Mg + Fe)) for spinels in the Murray Ridge peridotites (abyssal peridotite field is from Dick and Bullen (1984), whereas dunite, harzburgite, and plagioclase and spinel lherzolite spinels fields are from Burgath and Weiser (1980) and Leblanc et al. (1980)); (B) Al_2O_3 in orthopyroxene; and (C) Mg# in olivine for the Murray Ridge peridotites and peridotites from pre-oceanic rifts, abyssal peridotites, and subduction margins (modified from Bonatti and Michael 1989).

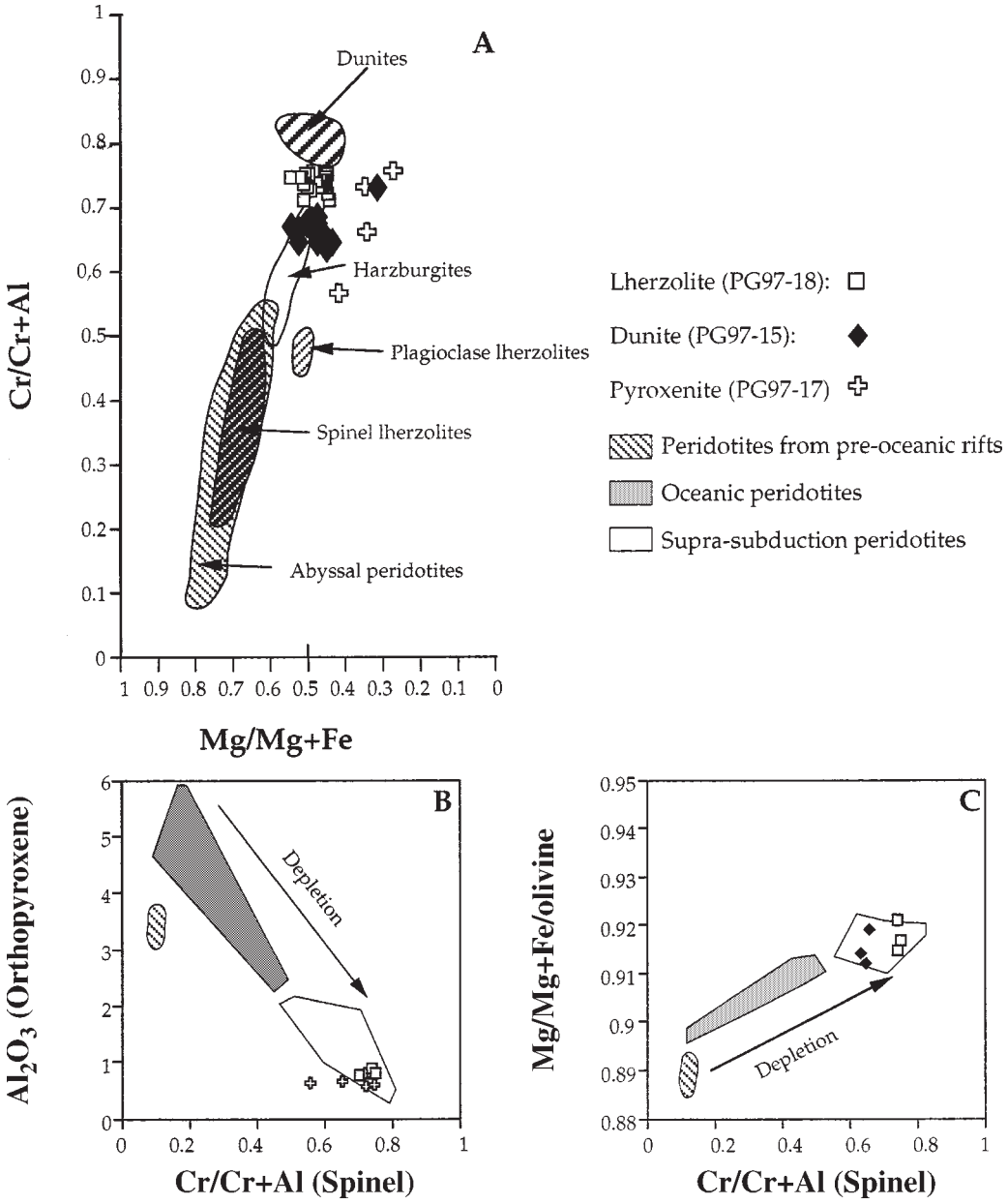

tive to PM (Fig. 8E). This suggests that these mafic rocks are geochemically similar to N-type MORB (N-MORB). However, the Nb and Ta enrichments (relative to PM) of the dolerite and basalt suggest that both rocks likely derive from a less depleted source than N-MORB. The gabbro differs from the basalt and dolerite by lower abundances in trace elements and marked Nb and Ti negative anomalies. The positive Eu and Sr anomalies of this gabbro reflect plagioclase accumulation. A dolerite (PG96-17) dyke from the Rubyrock igneous complex differs from PG96-12 and PG96-15 by a slightly higher $(La/Yb)_N$ ratio (0.64) and a small Nb and Ta depletion (relative to PM; Table 1).

The PM-normalized multielement diagrams for the foliated peridotites are presented in Fig. 8F. Some striking features in these patterns should be noted: (*i*) trace element contents of the peridotites are very low (< 1 time the PM abundances); (*ii*) the peridotites have positive Ba, Pb, and HREE anomalies; (*iii*) in contrast, Nb, Ta, and Zr have negative anomalies; and (*iv*) Rb, U, and Sr contents are variable.

The volcanic blocks of the Cache Creek Melange

Samples 95CC1 and 95CC4 are geochemically similar to Upper Triassic type 1 because of their flat patterns (1.27 < $(La/Yb)_N$ = 1.31) and Th negative anomalies (Fig. 10A). Their positive Sr anomaly reflects plagioclase accumulation.

Sample 99WL differs from samples 95CC1 and 95CC4 by

Table 3. Analytical data for selected igneous mafic rocks of the Cache Creek Melange from Cache Creek and Williams Lake.

Rock type:	Basalt	Basalt	Dolerite	Dolerite	Basalt	Basalt	Basalt	Basalt	Basalt
Sample No.:	95CC1	95CC4	99CC1	99CC2	99WL2	99WL3	99WL5	99WL6	99WL7
Cs			2.190	1.022	3.470	27.400	13.150	0.026	1.860
Rb	8.38	1.38	12.09	4.34	0.10	46.93	3.99	56.65	3.37
Sr	268.00	470.00	29.21	40.54	8.15	147.98	117.85	446.82	262.97
Ba	970.00	394.90	181.67	220.97	417.08	212.49	511.89	6408.81	206.77
U	0.26	0.41	0.05	0.04	1.05	0.40	0.30	5.15	0.42
Th	0.37	0.34	0.09	0.11	2.79	0.63	0.66	9.92	0.58
Pb	1.66	1.40	0.24	0.35	2.11	0.86	0.85	21.80	0.43
Hf	3.09	2.31	0.98	1.11	6.09	2.84	3.37	3.43	3.13
Zr	115.58	83.32	28.03	25.61	262.75	97.05	129.96	130.10	119.92
Ta	0.400	0.260	0.005	0.080	2.460	0.760	0.750	0.940	0.670
Nb	5.94	3.92	0.56	0.99	39.19	11.72	11.36	13.28	9.66
Y	33.22	29.45	20.63	28.64	28.35	39.61	31.53	29.77	28.34
La	5.71	4.80	1.37	2.28	25.80	12.27	8.99	29.01	7.48
Ce	16.12	11.64	4.57	7.38	61.14	31.16	22.82	57.00	19.55
Pr	2.65	1.93	0.82	1.30	8.00	4.48	3.32	6.91	2.92
Nd	13.29	9.50	4.55	7.11	33.52	21.10	15.49	25.61	13.88
Sm	4.31	3.19	1.74	2.56	7.15	5.79	4.35	5.10	4.01
Eu	1.44	1.09	0.68	0.93	2.45	2.11	1.60	1.61	1.48
Gd	4.99	3.86	2.51	3.58	6.77	7.07	5.36	5.60	4.90
Tb	0.87	0.72	0.47	0.68	0.95	1.16	0.89	0.79	0.81
Dy	5.47	4.59	3.12	4.32	5.30	7.34	5.41	4.67	4.95
Ho	1.21	1.06	0.72	0.99	0.98	1.43	1.16	1.01	1.01
Er	3.22	2.85	2.03	2.76	2.50	3.84	3.09	2.88	2.74
Tm	0.51	0.45	nd	nd	nd	nd	nd	nd	nd
Yb	3.12	2.71	1.95	2.67	1.88	3.02	2.71	2.91	2.37
Lu	0.48	0.41	0.30	0.41	0.26	0.42	3.37	0.45	0.35

Note: Analyses performed by ICP–MS at the Université Joseph Fourier, Grenoble, France.

lower trace element contents and LREE enrichment relative to HREE ($(La/Yb)_N$ = 2.27; $(La/Sm)_N$ = 1.20). This rock shows transitional characteristics between Triassic types 1 and 3.

Samples 99WL2, 99WL5, and 99WL6 have alkalic features characterized by high levels in high field strength elements (HFSE), have important LREE enrichments ($9.85 < (La/Yb)_N < 2.38$), and thus resemble Triassic type 3. The anomalous behaviour of Sr and Pb reflects the important alteration that affects these rocks.

Dolerites 99CC1 and 99CC2 are geochemically similar to the basalt and dolerite within the Pinchi Fault and show N-MORB affinities (Fig. 8E). Indeed, their PM normalized multielement plots have marked depletions in LREE ($0.49 < (La/Yb)_N < 0.84$), Zr, Hf, Nb, Ta, and Th (Fig. 10C). Moreover, 99CC1 has a very low trace element content (about 1.0 times the PM abundances).

This regional sampling indicates that both N-MORB tholeiites and plume-related tholeiitic and alkalic mafic lavas are found throughout the Cache Creek accretionary prism.

Nd and Sr isotopic compositions of the mafic and ultramafic rocks of the Cache Creek Terrane

Nd and Sr isotopic compositions have been determined for all the rock types exposed in the Fort St. James area, with the exception of the foliated peridotites. Whole rocks powders were leached in a 2N HCl – 0.1N Hf mixture. The $^{143}Nd/^{144}Nd$ and $^{87}Sr/^{86}Sr$ isotopic characteristics were determined on a Finnigan MAT261 multicollector mass spectrometer at the Université Paul Sabatier (Toulouse, France) using the analytical procedures of Lapierre et al. (1997). Results on La Jolla Nd standard yielded $^{143}Nd/^{144}Nd = 0.511850 \pm 8$ (mean on 39 runs), corresponding to an external reproducibility of 0.00001. Results on NBS 987 Sr standard yielded $^{87}Sr/^{86}Sr = 0.710250$ (mean on 200 runs).

All the isotopic data have been corrected for "in situ decay," with ages of 280 and 210 Ma for the mid-Permian and Upper Triassic lavas of the Cache Creek Complex, respectively. We assumed a 210 Ma age for the rocks exposed in the Pinchi Fault system on the basis of the 211–218 Ma K/Ar ages of the blueschists (K/Ar dating of phengitic muscovite; Paterson and Harakal 1974). White mica from these same blueschists was dated as 221–224 Ma using Ar^{40}–Ar^{39} (Ghent et al. 1996).

The $\varepsilon_{Nd(i)}$ ratios range between +9.1 and +2 and vary according to rock type. Permian icelandite and basalt, Triassic type 1 basalts, and igneous rocks within the Pinchi Fault have the highest $\varepsilon_{Nd(i)}$ ratios (+7.4 to +9.6; Table 1; Fig. 11), whereas those of type 3 alkali have the lowest (+2.0 to +5.3). The $\varepsilon_{Nd(i)}$ values of type 2 are intermediate between those of type 1 (~+7) and type 3 (~+4.9). Moreover, $\varepsilon_{Nd(i)}$ correlates negatively with $(Sm/Yb)_N$ (Fig. 11B). In contrast to what could be inferred from the trace elements, the type 1

Fig. 8. Primitive mantle normalized trace element patterns for the rocks of the Cache Creek Group and the Murray Ridge ultramafic rocks. Primitive mantle values are after Sun and McDonough (1989).

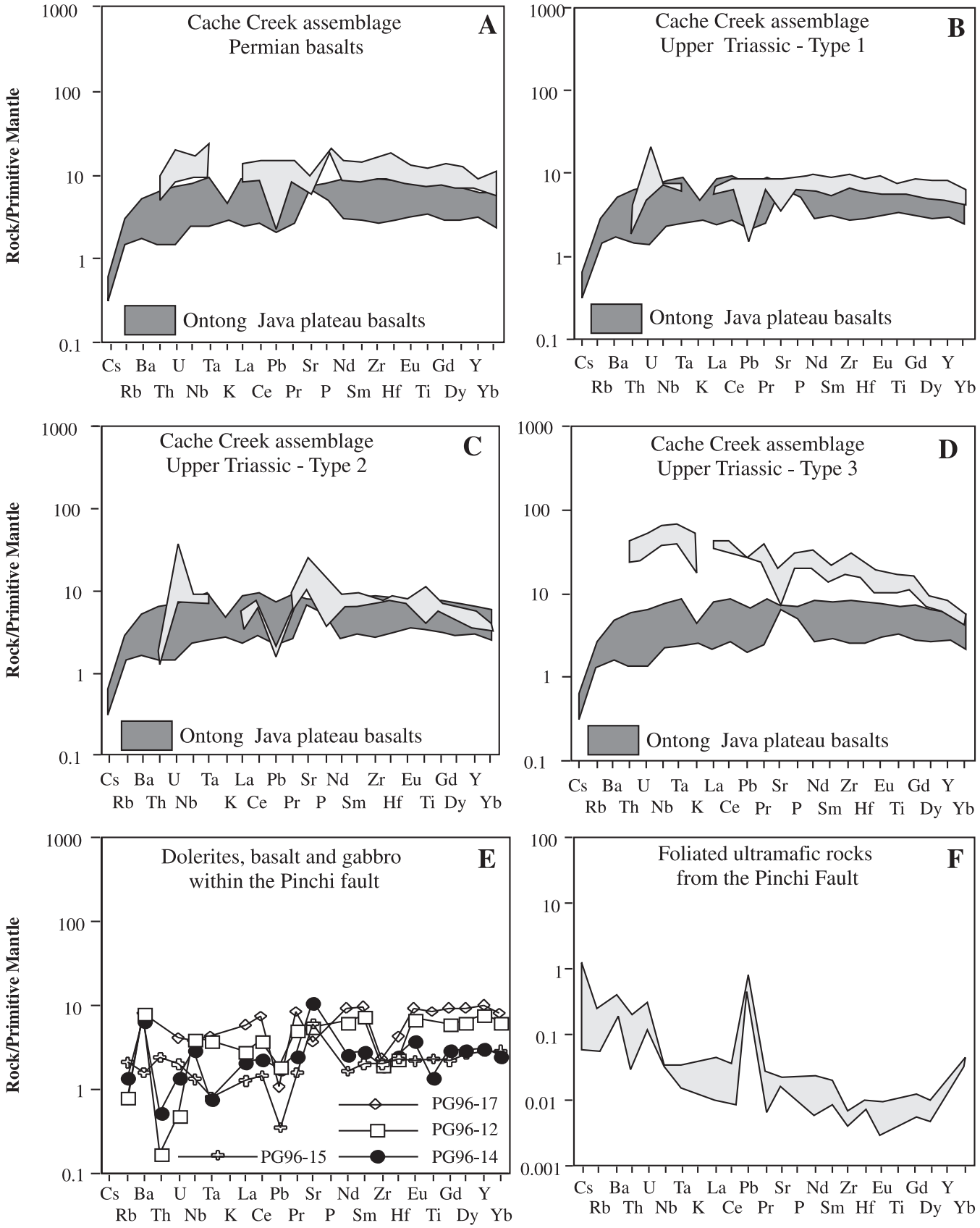

Fig. 9. Plots of (A) Zr/TiO_2 versus Nb/Y, (B) Zr/Y versus Zr/Nb, and (C) $(Dy/Yb)_N$ versus $(La/Yb)_N$ for the rocks of the Cache Creek Group and the mafic rocks within the Pinchi Fault Zone. Cretaceous basalts of the Caribbean–Colombian (Kerr et al. 1997) and Ontong Java plateaus (Neal et al. 1997) are given for comparison. The field of southern East Pacific Rise MORB (EPR-MORB) is after Mahoney et al. (1994).

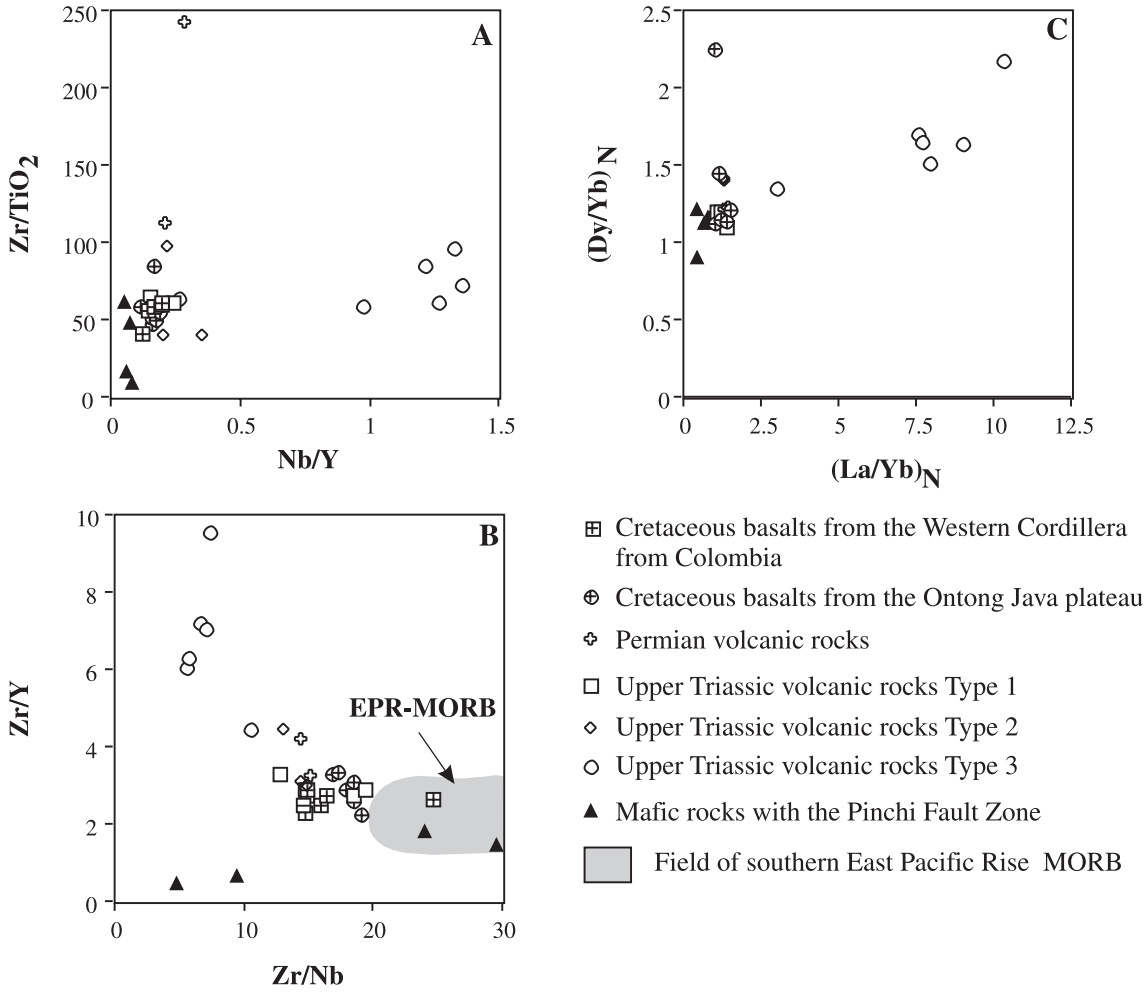

tholeiites have slightly higher $\varepsilon_{Nd(i)}$ values than the N-MORB-type basalt and dolerite within the Pinchi Fault system (PG96-12, PG96-15).

The ratio $(^{87}Sr/^{86}Sr)_i$ is highly variable and ranges from 0.70295 to 0.70830. The highest ratios are thought to reflect post-magmatic enrichment in radiogenic Sr related to hydrothermal alteration. The basalt (PG96-12), dolerite (PG96-15), and gabbro (PG96-14) within the Pinchi Fault system have lower $(^{87}Sr/^{86}Sr)_i$ values (0.70295–0.70300) and fall within the mantle array. We have mentioned in a previous section that these rocks were rather preserved from alteration. Thus, the $(^{87}Sr/^{86}Sr)_i$ of these rocks could reflect the isotopic composition of the mantle source (Fig. 10A).

In summary, mid-Permian and Upper Triassic types 1 and 2 are tholeiitic and type 3 is alkalic. The absence of Nb, Ta, and Ti negative anomalies and other features of subduction-related lavas and their Nd isotopic compositions suggest that this material was plume derived. Igneous rocks from the Pinchi Fault system differ from the Permian and Triassic lavas by LREE-depleted patterns and Th, Zr, and Hf negative anomalies. Cumulate gabbro differs from the dolerites and basalt by a marked Nb negative anomaly. Gabbro, dolerites, and basalt have high ε_{Nd} ratios which are similar to those of type 1. Foliated ultramafic rocks from the Pinchi Fault system display petrological and geochemical features of very depleted peridotites.

Discussion

The chemical data presented here can help resolve the tectonic setting of the Cache Creek mafic igneous components as either mid-oceanic ridge or oceanic plateau. These settings are discussed on the basis of their trace element and isotopic chemistry.

First, as Figs. 8–10 show, the mid-Permian and Upper Triassic volcanic rocks of the Sowchea succession and Cache Creek Melange display features of plume-related magma. All these volcanic rocks have La/Nb ratios consistently less than 2 (Tables 1, 3), except for samples 99CC1 and 99CC2, which have higher La/Nb ratios (~2.4). Type 1 is geochemically similar to the Ontong Java oceanic plateau basalts (Fig. 8B). The mid-Permian tholeiite and Upper Triassic type 2 share with the Ontong Java oceanic plateau basalt similar flat

multielement plots. However, the mid-Permian volcanic rocks differ from the Ontong Java oceanic plateau basalt by higher trace element abundances and the marked LREE depletion of type 2 is absent in oceanic plateau basalts. Finally, the Zr/Nb ratios of the Cache Creek tholeiites fall in the restricted range (between 15 and 20) of the basalt from Ontong Java and Colombia (Fig. 10B) and are consistent with high degrees of partial melting. The depletion in HREE and Y and the high $(Dy/Yb)_N$ and $(La/Yb)_N$ of the Upper Triassic alkali type 3 (relative to types 1 and 2; Fig. 10) indicate the presence of residual garnet in the lherzolite source.

Second, the variations in Nd isotope and incompatible trace elements (Fig. 11; Tables 1, 3) indicate that these lavas may have been generated from a heterogeneous plume or the mixing of depleted N-MORB and enriched OIB sources. Indeed, Triassic type 1 and igneous rocks from the Pinchi Fault system have altogether the lowest LREE abundances and the highest $\varepsilon_{Nd(i)}$ values which are in the range of N-MORB or in the common field of N-MORB and OIB. In contrast, Triassic type 3 rocks have the highest LREE contents and the lowest $\varepsilon_{Nd(i)}$ which fall in the OIB field. Finally, Triassic type 2 rocks have geochemical and Nd isotopic compositions which are intermediate between types 1 and 3 and their ε_{Nd} values fall in the range of OIB. Assuming that the rocks from the Pinchi Fault system are the same age as the Cache Creek Upper Triassic lavas, the most likely geodynamic environment of the Cache Creek oceanic terrane is a near-ridge or ridge-centred oceanic plateau.

By contrast with most Cache Creek exposures, some rocks show distinct origin, especially the foliated ultramafic rocks. The tectonic setting of foliated pyroxenite is difficult to determine because it has been seldom described in the literature. The foliated ultramafic rocks from Murray Ridge are geochemically similar to very depleted harzburgite and dunite (Parkinson and Pearce 1998; Garrido and Bodinier 1999). However, they differ from depleted abyssal harzburgite because clinopyroxene represents the predominant phase. The compositions of their Cr spinels are similar to those of peridotite from Conical Seamount located in the Izu–Bonin–Mariana forearc (Parkinson and Pearce 1998). However, their paragenesis is very different because diopside represents the predominant phase. Foliated and very depleted pyroxenite associated with deformed dunite and lherzolite have been described in the Ronda massif and the Jilal complex (Kohistan Complex, Pakistani Himalaya), interpreted to represent an infra-arc crust–mantle transition (Burg et al. 1998; Garrido and Bodinier 1999). In both complexes, Al_2O_3 of diopside is very low (even lower in the Murray Ridge peridotites; Table 2), and primitive mantle trace element plots of pyroxenite show enrichments in Rb and Ba and have very low contents in HREE (<0.1 times the PM values). Moreover, Cr spinels of the Murray Ridge ultramafic rocks plot within the subduction zone related field (Fig. 7). However, Murray Ridge ultramafic rocks differ from Ronda pyroxenite by higher concentrations of Pb and Cr-poor clinopyroxene. Pyroxenites from Ronda massif and Jilal complex are interpreted to result from metasomatic reaction between melt and peridotite at pressure–temperature (*P–T*) conditions close to the peridotite solidus. During cool-

Fig. 10. Primitive mantle normalized trace element patterns for the volcanic blocks caught in the melange near the Cache Creek Complex type locality. Primitive mantle values are after Sun and McDonough (1989).

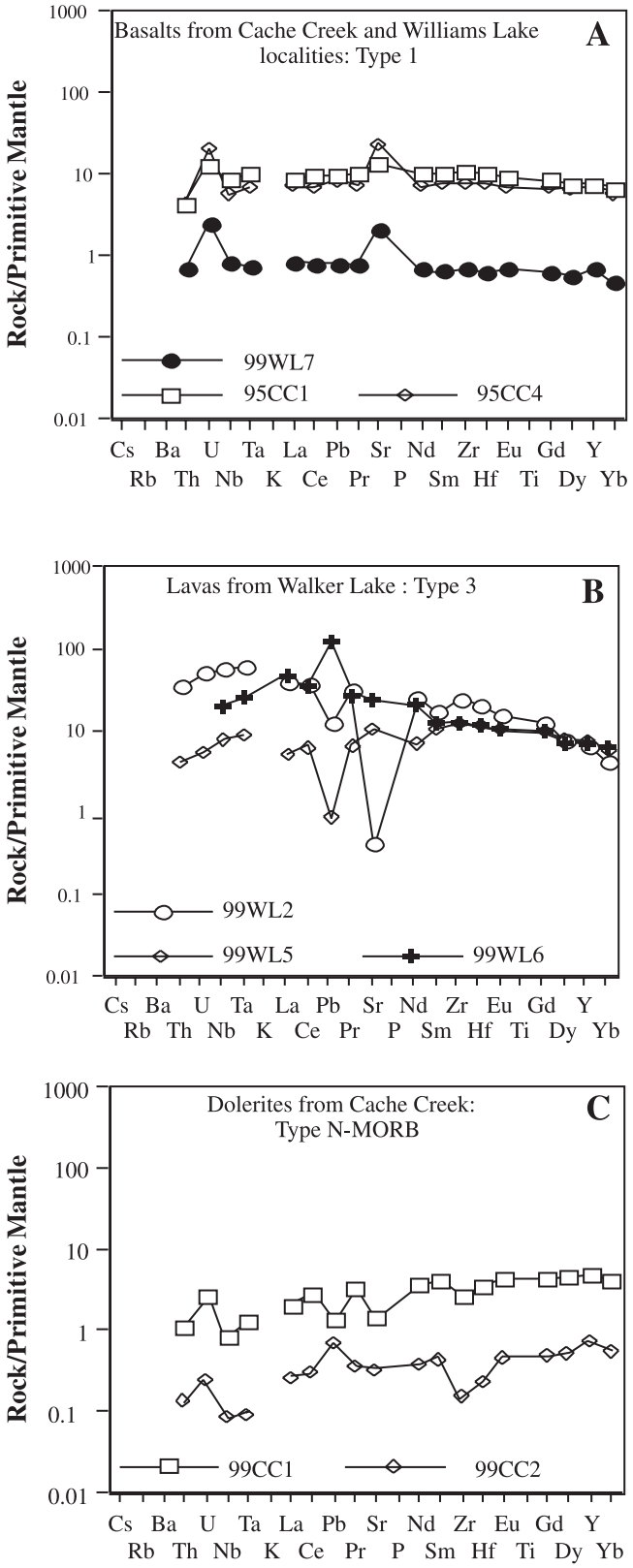

Fig. 11. $\varepsilon_{Nd(i)}$ versus (A) $(^{87}Sr/^{86}Sr)_i$ and (B) $(Sm/Yb)_N$ correlation plots for the igneous rocks of the Cache Creek Group. MORB and OIB fields are after DePaolo (1988).

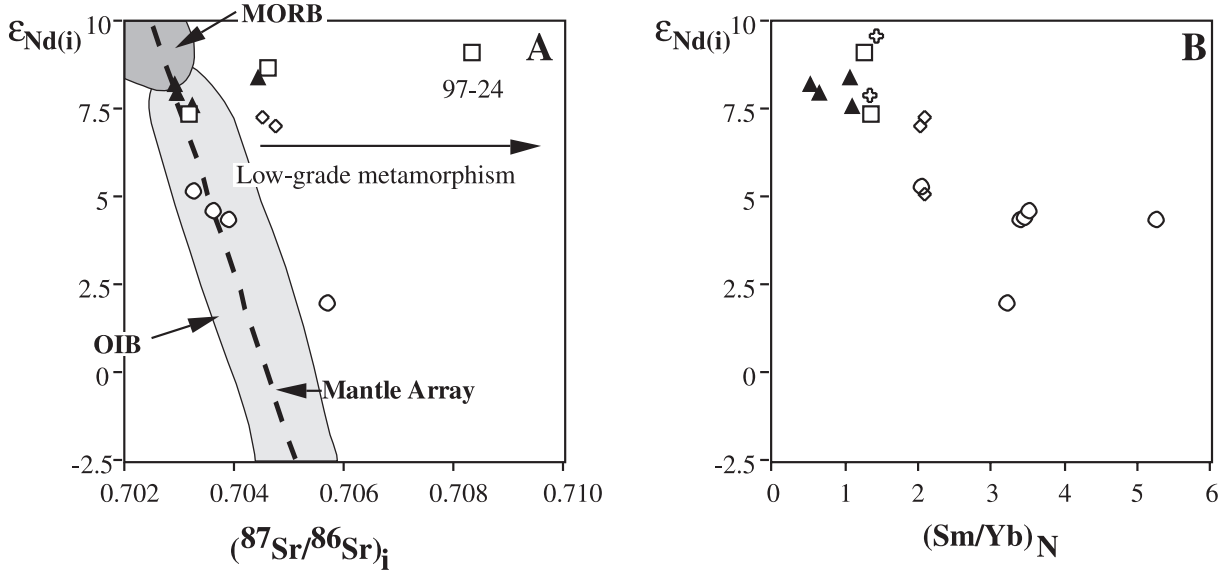

Permian lavas

Upper Triassic lavas Type 1

Upper Triassic lavas Type 2

Upper Triassic lavas Type 3

Mafic rocks caught in the Pinchi Fault

ing, interstitial melts become saturated in pyroxene and react with olivine to produce secondary clinopyroxene and orthopyroxene (Burg et al. 1998; Garrido and Bodinier 1999). Thus, the Murray Ridge refractory pyroxenite and associated dunite and lherzolite could represent the depleted upper mantle of the Quesnel arc crust, exhumed during (*i*) the collision of the Cache Creek oceanic plateau with the Quesnel arc and the deformation of the arc and the accretionary prism, or (*ii*) the emplacement of the Tertiary Pinchi strike-slip fault.

Proposed geodynamic environment for the Cache Creek accretionary prism

A simplified geodynamic model for the Cache Creek oceanic suture is shown in Fig. 12.

During the Permian, the geodynamic environment was probably an oceanic realm where oceanic islands and carbonate platforms developed, the remnants of which are the mid-Permian oceanic island tholeiites and the Copley reef limestone (Struik et al. 2001). At the same time, subduction occurred to the east, leading to the development of the Quesnellia arc (Monger and Ross 1971; Nelson and Mihalynuk 1993).

During the Late Triassic, Permian rocks began to subduct, leading to the development of an accretionary prism and high-pressure, low-temperature metamorphism. Offshore, vast outpourings of plume-related basaltic magma occurred, thickening the Permian oceanic crust and leading to the creation of an oceanic plateau. The incompatible trace element and Nd isotopic compositions of the Cache Creek Upper Triassic mafic lavas and the igneous rocks from the along the Pinchi Fault, which likely represent the remnants of this oceanic plateau, indicate that magmatism likely took place in a ridge-centered or near-ridge hotspot.

During the Early Jurassic, this overthickened oceanic crust reached the accretionary prism, its anomalous thickness probably hindered its subduction under the Quesnellia arc, and part of this oceanic plateau was obducted on or accreted to the Quesnellia arc terrane and its accretionary prism.

During the Tertiary (Eocene), the dextral Pinchi shear fault system caused (*i*) the deformation of the accreted Permian to Triassic exotic rocks, the Quesnellia arc terrane and its related accretionary prism; and (*ii*) the exhumation of the deepest roots of the arc crust (Murray Ridge foliated ultramafic rocks) and related prism (Upper Triassic blueschists).

Acknowledgments

This work was funded by the Centre National de la Re-

Fig. 12. Cartoon illustrating the geodynamic evolution of the Cache Creek oceanic domain from the Permian up to the Late Triassic.

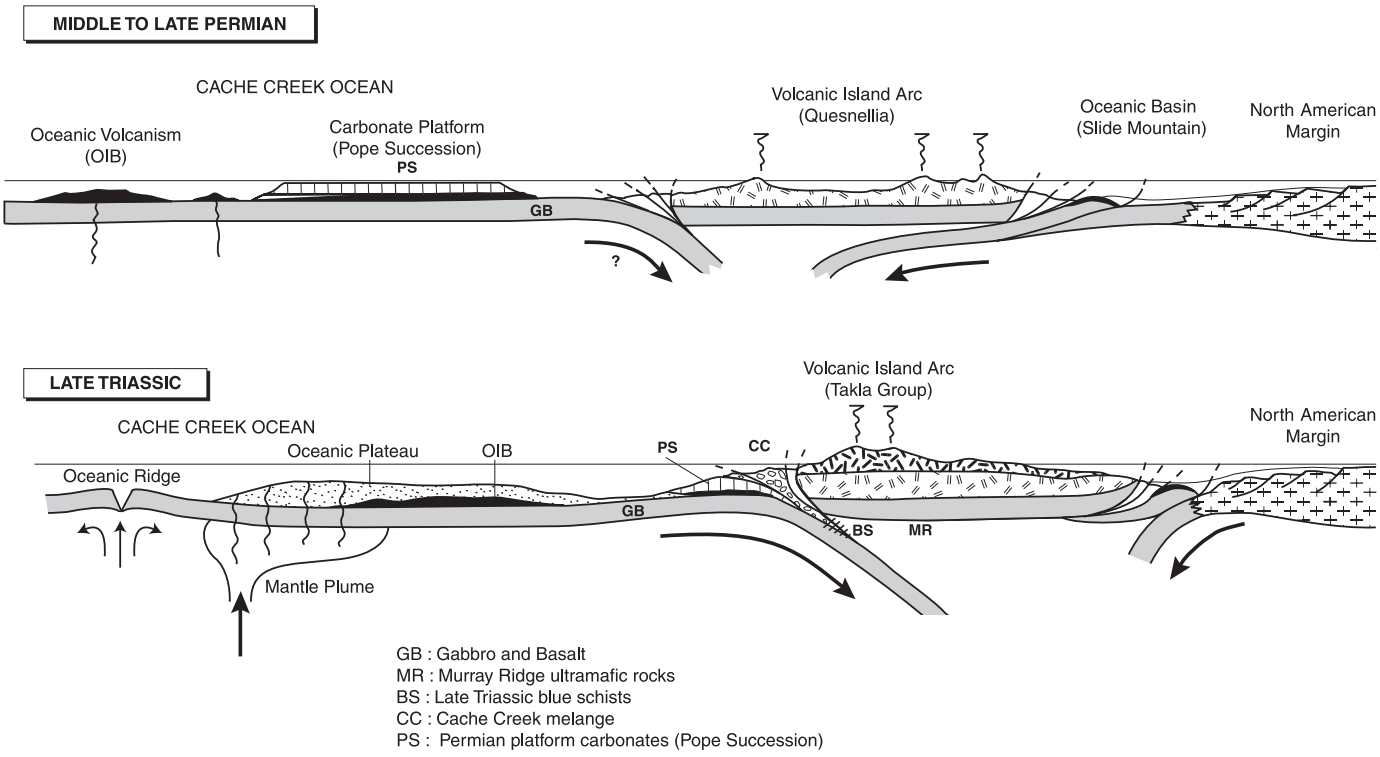

cherche Scientifique teams UMR 5025 and Université de Savoie and has benefited from Ministère de l'Education Nationale et de la Recherche DSPT3 grants to H. Lapierre. Field expenses were supported by the Nechako NATMAP Project. We would like to thank J. Ann Nelson and I. Parkinson for their helpful reviews.

References

Armstrong, J.E. 1949. Fort St. James map-area, Cassiar and Coast Districts, British Columbia. Geological Survey of Canada, Memoir 252.

Arai, S. 1994. Characterization of spinel peridotites by olivine–spinel composition relationships: review and interpretation. Chemical Geology, **113**: 191–204.

Barrat, J.-A., Keller, F., Amossé, J., Taylor, R.N., Nesbitt, R.W., and Hirata, T. 1996. Determination of rare earth elements in sixteen silicate reference samples by ICP-MS using a Tm addition and an ion-exchange chromatography procedure. Geostandards Newsletter, **20**: 133–139.

Bonatti, E., and Michael, P.J. 1989. Mantle peridotites from continental rifts to ocean basins to subduction zones. Earth and Planetary Science Letters, **91**: 297–311.

Burg, J.-P., Bodinier, J.-L., Chaudhry, S., Hussain, S., and Dawood, H. 1998. Infra-arc mantle–crust transition and intra-arc mantle diapirs in the Kohistan Complex (Pakistani Himalaya): petrostructural evidence. Terra Nova, **10**: 74–80.

Burgath, K., and Weiser, T. 1980. Primary features and genesis of Greek podiform chromite deposits. *In* Ophiolites, Proceedings of the International Ophiolite Symposium, Nicosia, Cyprus, 1979. *Edited by* A. Panayiotou. Ministry of Agriculture and Natural Resources, Geological Survey, Republic of Cyprus, pp. 675–690.

Childe, F.C., and Schiarizza, P. 1997. U–Pb geochronology and Nd isotopic systematics of the Sitlika assemblage, central British Columbia. *In* Geological fieldwork 1996. British Columbia Ministry of Employment and Investment, Paper 1997-1, pp. 69–77.

Cordey, F., and Struik, L.C. 1996. Radiolarian biostratigraphy and implications, Cache Creek Group of Fort Fraser and Prince George map areas, central British Columbia. *In* Current research 1996-E. Geological Survey of Canada, Paper 1996-E, pp. 7–18.

DePaolo, D.J. 1988. Neodymium isotope geochemistry, an introduction, minerals and rocks. Springer Verlag, Berlin.

Dick, H.J.B., and Bullen, T. 1984. Chromium spinel as petrogenetic indicator in abyssal alpine-type peridotites and spatially associated lavas. Contributions to Mineralogy and Petrology, **86**: 54–76.

Gabrielse, H., and Yorath, C.J. 1991. Tectonic synthesis. *In* Geology of the Cordilleran Orogen in Canada. *Edited by* H. Gabrielse and C.J. Yorath. Geological Survey of Canada, Geology of Canada, No. 4, Chap. 18, pp. 677–705.

Garrido, C.J., and Bodinier, J.-L. 1999. Diversity of mafic rocks in

the Ronda Peridotite: evidence for pervasive melt–rock reaction during heating of subcontinental lithosphere by upwelling asthenosphere. Journal of Petrology, **40**: 729–754.

Ghent, E.D., Erdmer, P., Archibald, D.A., and Stout, M.Z. 1996. Pressure–temperature and tectonic evolution of Triassic lawsonite–aragonite blueschists from Pinchi Lake, British Columbia. Canadian Journal of Earth Sciences, **33**: 800–810.

Kerr, A.C., Marriner, G.F., Tarney, J., Nivia, A., Saunders, A.D., Thirlwall, M.F., and Sinton, C.W. 1997. Cretaceous basaltic terranes in western Colombia; elemental, chronological and Sr–Nd isotopic constraints on petrogenesis. Journal of Petrology, **38**: 677–702.

Lapierre, H., Dupis, V., Mercier de Lépinay, B., Tardy, M., Ruiz, J., Maury, R.C., Hernandez, J., and Loubert, M. 1997. Is the Lower Duarte Igneous Complex (Hispaniola) a remnant of the Carribean plume generated oceanic plateau? Journal of Geology, **105**: 111–120.

Leblanc, M., Dupuy, C., Cassard, D., Moutte, J., Nicolas, A., Prinzhoffer, A., Rabinovitch, M., and Routhier, P. 1980. Essai sur la genèse des corps podiformes de chromite dans les péridotites ophiolithiques: étude des chromites de Nouvelle Calédonie et comparaison avec celles de Méditerranée orientale. *In* Ophiolites, Proceedings of the International Ophiolite Symposium, Nicosia, Cyprus, 1979. *Edited by* A. Panayiotou. Ministry of Agriculture and Natural Resources, Geological Survey, Republic of Cyprus, pp. 691–70.

Mahoney, J.J., Sinton, J.M., Kurz, M.D., Macdougall, J.D., Spencer, K.J., and Lugmuir, G.W. 1994. Isotope and trace element characteristics of a super-fast spreading ridge: East Pacific Rise, 13°–23°S. Earth and Planetary Science Letters, **121**: 173–194.

Mihalynuk, M.G., Nelson, J.-A., and Diakow, L.J. 1994. Cache Creek terrane entrapment: oroclinal paradox within the Canadian Cordillera. Tectonics, **13**: 575–595.

Monger, J.W.H. 1975. Upper Paleozoic rocks of the Atlin Terrane, northwestern British Columbia and south-central Yukon. Geological Survey Canada, Paper 74-47.

Monger, J.W.H., and Ross, C.A. 1971. Distribution of fusulinaceans in the Western Canadian Cordillera. Canadian Journal of Earth Sciences, **8**: 259–278.

Monger, J.W.H., Gabrielse, H., and Souther, J.A. 1972. Evolution of the Canadian Cordillera: a plate tectonic model. American Journal of Science, **272**: 577–602.

Morimoto, N. 1988. Nomenclature of pyroxenes. Schweizerische Mineralogische und Petrographische Mitteilungen, **68**: 95–111

Neal, C.R., Mahoney, J.J., Kroenke, L.W., Duncan, R.A., and Petterson, M.G. 1997. The Ontong Java oceanic plateau. *In* Large igneous provinces. *Edited by* J.J. Mahoney and M. Coffin. Continental, Oceanic, and Planetary Flood Volcanism American Geophysical Union Monograph 100, pp. 183–216.

Nelson, J.A., and Mihalynuk, M. 1993. Cache Creek ocean: closure or enclosure? Geology, **21**: 173–176.

Orchard, M.J., Struik, L.C., and Taylor, H. 1998. New conodont data from the Cache Creek Group, central British Columbia. *In* Current research 1998-A. Geological Survey of Canada, Paper 1998-A, pp. 99–105.

Orchard, M.J., Struik, L.C., Rui, L., Bamber, E.W., Mamet, B., Struik, L.C., Sano, H., and Taylor, H. 2001. Paleontological and biogeographical constraints on the Carboniferous to Jurassic Cache Creek Terrane in central British Columbia. Canadian Journal of Earth Sciences, **38**(4): 551–578.

Parkinson, I.J., and Pearce, J.A. 1998. Peridotites from the Izu–Bonin–Mariana Forearc (ODP Leg 125): evidence for mantle melting and melt–mantle interaction in a supra-subduction zone setting. Journal of Petrology, **39**: 1577–1618.

Paterson, I.A. 1973. The geology of the Pinchi Lake area, central British Columbia. Ph.D. thesis, University of British Columbia, Vancouver, B.C.

Paterson, I.A. 1974. Geology of Cache Creek Complex and Mesozoic rocks at the northern end of the Stuart Lake Belt, Central British Columbia. *In* Report of activities, part B. Geological Survey of Canada, Paper 74-1B, pp. 31–42.

Paterson, I.A., and Harakal, J.E. 1974. Potassium–argon dating of blueschists from Pinchi Lake, central British Columbia. Canadian Journal of Earth Sciences, **7**: 1007–1011.

Schiarizza, P., Massey, N., and MacIntyre, D.G. 1998. Geology of the Sitlika Assemblage in the Takla Lake area (93 N/3, 4, 5, 6, 12), central British Columbia. *In* Geological fieldwork 1997. British Columbia Ministry of Employment and Investment, Paper 1998-1, pp. 4-1–4-20.

Souther, J.G. 1991. Régimes volcaniques dans Géologie de l'orogène des Cordillères au Canada. *In* Geology of the Cordilleran Orogen in Canada. *Edited by* H. Gabrielse and C.J. Yorath. Geological Survey of Canada, Geology of Canada, No. 4, pp. 501–536.

Struik, L.C., Floriet, C., and Cordey, F. 1996. Geology near Fort St. James, central British Columbia. *In* Current research 1996-A. Geological Survey of Canada, Paper 1996-A, pp. 71–76.

Struik, L.C., Schiarizza, P., Orchard, M.J., Cordey, F., Sano, H., MacIntyre, D.G., Lapierre, H., and Tardy, M. 2001. Imbricate architecture of upper Paleozoic to Jurassic oceanic Cache Creek Terrane, central British Columbia. Canadian Journal of Earth Sciences, **38**(4): 495–514.

Sun, S.-S., and McDonough, W.F. 1989. Chemical and isotopic of oceanic basalts: implications for mantle composition and processes. *In* Magmatism in the ocean basins. *Edited by* A.D. Saunders and N.J. Norry. Geological Society Special Publication (London), No. 42, pp. 313–345.